














## Improved Constraints on the Recent Terrestrial Carbon Sink Over China by Assimilating OCO-2 XCO<sub>2</sub> Retrievals

Wei He<sup>1,2</sup> , Fei Jiang<sup>1,2,3</sup> , Weimin Ju<sup>1,2</sup> , Frédéric Chevallier<sup>4</sup> , David F. Baker<sup>5</sup>, Jun Wang<sup>1,2</sup> , Mousong Wu<sup>1,2</sup> , Matthew S. Johnson<sup>6</sup> , Sajeep Philip<sup>7</sup> , Hengmao Wang<sup>1,2</sup> , Michael Bertolacci<sup>8</sup> , Zhiqiang Liu<sup>9</sup> , Ning Zeng<sup>9,10</sup> , and Jing M. Chen<sup>11,12</sup> 

<sup>1</sup>International Institute for Earth System Science, Nanjing University, Nanjing, China, <sup>2</sup>Jiangsu Provincial Key Laboratory of Geographic Information Science and Technology, Key Laboratory for Land Satellite Remote Sensing Applications of Ministry of Natural Resources, School of Geography and Ocean Science, Nanjing University, Nanjing, China, <sup>3</sup>Frontiers Science Center for Critical Earth Material Cycling, Nanjing University, Nanjing, China, <sup>4</sup>Laboratoire des Sciences du Climat et de L'Environnement, LSCE/IPSL, CEA-CNRS-UVSQ, Université Paris-Saclay, Gif-sur-Yvette, France, <sup>5</sup>Cooperative Institute for Research in the Atmosphere, Colorado State University, Fort Collins, CO, USA, <sup>6</sup>Earth Science Division, NASA Ames Research Center, Moffett Field, CA, USA, <sup>7</sup>Centre for Atmospheric Sciences, Indian Institute of Technology Delhi, New Delhi, India, <sup>8</sup>School of Mathematics and Applied Statistics, University of Wollongong, Wollongong, NSW, Australia, <sup>9</sup>Laboratory of Numerical Modeling for Atmospheric Sciences & Geophysical Fluid Dynamics, Institute of Atmospheric Physics, Chinese Academy of Sciences, Beijing, China, <sup>10</sup>Earth System Science Interdisciplinary Center, College Park, MD, USA, <sup>11</sup>Department of Geography and Planning, University of Toronto, Toronto, ON, Canada, <sup>12</sup>School of Geographical Sciences, Fujian Normal University, Fuzhou, China

### Special Section:

Carbon Weather: Toward the next generation of regional greenhouse gas inversion systems

### Key Points:

- Orbiting Carbon Observatory 2 (OCO-2) inversions reveal the largest carbon sink in China is in the south on an annual basis, while in the northeast during peak growing season
- The seasonal cycle appears to be well constrained in the monsoon climate zones
- OCO-2 inversions are able to capture the impacts of climate extremes on China's carbon sink interannual variability

### Supporting Information:

Supporting Information may be found in the online version of this article.

### Correspondence to:

F. Jiang,  
jiangf@nju.edu.cn

### Citation:

He, W., Jiang, F., Ju, W., Chevallier, F., Baker, D. F., Wang, J., et al. (2023). Improved constraints on the recent terrestrial carbon sink over China by assimilating OCO-2 XCO<sub>2</sub> retrievals. *Journal of Geophysical Research: Atmospheres*, 128, e2022JD037773. <https://doi.org/10.1029/2022JD037773>

Received 1 SEP 2022

Accepted 4 JUL 2023

### Author Contributions:

**Conceptualization:** Wei He, Fei Jiang

**Data curation:** Sajeep Philip

**Formal analysis:** Wei He

**Methodology:** Wei He

**Project Administration:** Fei Jiang

**Resources:** Weimin Ju, Frédéric Chevallier, David F. Baker, Matthew S. Johnson, Michael Bertolacci, Zhiqiang Liu, Ning Zeng

**Supervision:** Fei Jiang, Jing M. Chen

**Validation:** Fei Jiang

**Writing – original draft:** Wei He

**Abstract** The magnitude and distribution of China's terrestrial carbon sink remain uncertain due to insufficient observational constraints; satellite column-average dry-air mole fraction carbon dioxide (XCO<sub>2</sub>) retrievals may fill some of this gap. Here, we estimate China's carbon sink using atmospheric inversions of the Orbiting Carbon Observatory 2 (OCO-2) XCO<sub>2</sub> retrievals within different platforms, including the Global Carbon Assimilation System (GCAS) v2, the Copernicus Atmosphere Monitoring Service, and the OCO-2 Model Inter-comparison Project (MIP). We find that they consistently place the largest net biome production (NBP) in the south on an annual basis compared to the northeast and other main agricultural areas during peak growing season, coinciding well with the distribution of forests and crops, respectively. Moreover, the mean seasonal cycle amplitude of NBP in OCO-2 inversions is obviously larger than that of biosphere model simulations and slightly greater than surface CO<sub>2</sub> inversions. More importantly, the mean seasonal cycle of the OCO-2 inversions is well constrained in the temperate, tropical, and subtropical monsoon climate zones, with better inter-model consistency at a sub-regional scale compared to in situ inversions and biosphere model simulations. In addition, the OCO-2 inversions estimate the mean annual NBP in China for 2015–2019 to be between 0.34 (GCASv2) and 0.47 ± 0.16 PgC/yr (median ± std; OCO-2 v10 MIP), and indicate the impacts of climate extremes (e.g., the 2019 drought) on the interannual variations of NBP. Our results suggest that assimilating OCO-2 XCO<sub>2</sub> retrievals is crucial for improving our understanding of China's terrestrial carbon sink regime.

**Plain Language Summary** The magnitude and distribution of China's terrestrial carbon sink remain underconstrained; satellite column-average dry-air mole fraction carbon dioxide (XCO<sub>2</sub>) retrievals from NASA's Carbon Observatory 2 (OCO-2) could help reduce this uncertainty. This study revisited China's terrestrial carbon sink estimates based on state-of-the-art OCO-2 XCO<sub>2</sub> inversions, including the Global Carbon Assimilation System OCO-2 inversion, the Copernicus Atmosphere Monitoring Service OCO-2 inversion, and those in the OCO-2 Model Inter-comparison Project. We found that the assimilation of OCO-2 XCO<sub>2</sub> retrievals offers effective constraints on the spatiotemporal patterns of the terrestrial carbon sink of China. This result suggests that the OCO-2 XCO<sub>2</sub> inversions allow an improved understanding of China's land carbon sink over in situ CO<sub>2</sub> inversions and bottom-up biosphere model simulations, including better representations in spatial distributions and seasonal cycles and more plausible interannual variations. These improvements suggest that the assimilation of OCO-2 XCO<sub>2</sub> retrievals offers effective constraints on the spatiotemporal patterns of the terrestrial carbon sink of China.

**Writing – review & editing:** Fei Jiang, Weimin Ju, Frédéric Chevallier, David F. Baker, Jun Wang, Mousong Wu, Matthew S. Johnson, Sajeev Philip, Hengmao Wang, Michael Bertolacci, Zhiqiang Liu, Ning Zeng, Jing M. Chen

## 1. Introduction

The global terrestrial carbon sink offsets approximately one-third of the CO<sub>2</sub> emitted to the atmosphere by anthropogenic activities (Friedlingstein et al., 2022), thus playing an important role in the global carbon budget. While the global terrestrial carbon sink is relatively well quantified (about  $3.4 \pm 0.9$  PgC/yr) (Friedlingstein et al., 2022), the carbon sinks over different regions of the globe face large uncertainties. This is particularly true for regions where observational data is lacking, making it challenging for countries to evaluate the impact of their carbon-reduction measures. Thus, accurate quantification of carbon sinks requires further research attention at regional scales.

Atmospheric inversion is a significant approach to estimating surface carbon fluxes at global to regional scales and has been widely used for quantifying terrestrial carbon sinks (Chevallier et al., 2009; Peters et al., 2007; Peylin et al., 2013; Rödenbeck et al., 2003; van der Laan-Luijkx et al., 2017). In atmospheric inversions, the major sources of uncertainty in the carbon flux estimates are due to transport model errors, the quality and quantity (and distribution) of atmospheric CO<sub>2</sub> concentration measurements, inversion techniques, and, for regional inversion models, boundary condition errors (W. He et al., 2018b; Peylin et al., 2013). Therefore, it's essential to inter-compare transport models (e.g., TRANSCOM) (Gurney et al., 2004) and different inversion frameworks (e.g., in Orbiting Carbon Observatory [OCO]-2 Model Inter-comparison Project [MIP]) (Crowell et al., 2019; Peiro et al., 2022), and conduct regional carbon budget assessments (e.g., RECCAP-II) (Ciais et al., 2022) to better understand the uncertainties in carbon flux estimation at large scales. Recently, more attention has been given to regional scales (Ciais et al., 2022; Monteil et al., 2020; Philip et al., 2022), where quantification of terrestrial carbon sinks using atmospheric CO<sub>2</sub> data at regional scales is very meaningful for countries and smaller regions to assess their land sink capacity and make policy decisions regarding their respective carbon emissions.

However, quantifying the terrestrial carbon sink at regional scales poses significant challenges. Historically, disputes over the land carbon sink size of North America or the United States (Fan et al., 1998; Field & Fung, 1999; Holland & Brown, 1999) have been recently illuminated by decades of effort (Second State of the Carbon Cycle Report (SOCCR2, Cavallaro et al., 2018)). Similarly, ongoing debates persist over Europe's carbon sink size (Janssens et al., 2003; Reuter et al., 2017; Scholze et al., 2019). China faces similar issues, with fewer observational constraints available despite being the world's largest emitter of carbon. The Chinese government has set a goal of carbon neutrality and the paths toward this goal, where the terrestrial carbon sink plays a pivotal role in this issue. However, sparse CO<sub>2</sub> observational networks have made estimating China's terrestrial carbon sink highly uncertain. A large range of magnitudes (0.2–1.1 PgC/yr) for China's terrestrial carbon sink has been reported by different studies using atmospheric inversions (Jiang et al., 2016; Piao et al., 2009; Thompson et al., 2016; Yang et al., 2022). A recent study by J. Wang et al. (2020) reports China's carbon sink to be  $1.11 \pm 0.38$  PgC/yr over 2010–2016, which is thought likely to be an overestimate (Piao et al., 2022). Thus, accurately quantifying the terrestrial carbon sink over China is of great importance.

In recent years, satellite column-average dry-air mole fraction carbon dioxide (XCO<sub>2</sub>) has shown great promise to enhance the observational coverage of CO<sub>2</sub>. Atmospheric inversions of XCO<sub>2</sub> have been successfully used to constrain the terrestrial carbon sink over various regions of the globe (Jiang et al., 2021; J. Liu et al., 2021; R. Liu et al., 2021; Philip et al., 2022; H. Wang et al., 2019). Satellite XCO<sub>2</sub> is especially useful for regions lacking surface CO<sub>2</sub> data, such as China. The OCO-2 and more recently the OCO-3 satellites are of particular significance, providing high spatial resolution of XCO<sub>2</sub>. With a much smaller footprint size than the Greenhouse gases Observing Satellite (GOSAT), OCO-2 collects about 100 times more samples per day (Crisp et al., 2022), offering greater data density and less spatially mixed atmospheric signals. Therefore, OCO-2 has potential to provide new insights into understanding carbon sources or sinks at regional scales (Philip et al., 2022). Previous studies have utilized OCO-2 based inversions to investigate regional carbon budgets using either global (Philip et al., 2022) or regional models (Villalobos et al., 2021), and their seasonal cycle and interannual variability (IAV) (Z. Chen, Huntzinger, et al., 2021; Z. Chen, Liu, et al., 2021; Peiro et al., 2022; Villalobos et al., 2022) and extreme climate impacts (Crowell et al., 2019; Kwon et al., 2021) over regions such as Australia, South Asia, and Siberia. However, such research on China is relatively scarce.

In this study, we assess the magnitude and distribution of China's terrestrial carbon sink based on an ensemble of OCO-2 XCO<sub>2</sub> inversions, including the Global Carbon Assimilation System (GCAS) OCO-2 inversion, the Copernicus Atmosphere Monitoring Service (CAMS) OCO-2 inversion, and those inversions in the OCO-2 MIP

(OCO-2 v9 MIP and v10 MIP). We expect that the imposed constraints from OCO-2 XCO<sub>2</sub> retrievals should help to improve our understanding of the spatiotemporal characteristics of China's terrestrial carbon sink.

## 2. Data and Method

### 2.1. Global Carbon Assimilation System, Version 2

GCAS was originally developed in China in 2015 to assimilate in situ CO<sub>2</sub> data (S. Zhang et al., 2015). Recently it has been updated with a new scheme to assimilate satellite XCO<sub>2</sub> retrievals (Jiang et al., 2021). The system uses the atmospheric transport Model for OZone And Related chemical Tracers (MOZART-4) (Emmons et al., 2010), which is driven by the Goddard Earth Observing System Model, Version 5 (GEOS-5) meteorological fields and the Ensemble Square Root Filter optimization technique (Whitaker & Hamill, 2002). The GEOS-5 meteorological fields have a horizontal resolution of approximately 1.9° × 2.5° and 72 vertical layers. MOZART-4 was run with the same spatial resolution as GEOS-5, but with 56 vertical levels. The length of the data assimilation (DA) window is 1 week. In each DA window, a “two-step” calculation scheme is implemented in GCAS. First, the prior fluxes are optimized using XCO<sub>2</sub> data, then the optimized fluxes are fed into the MOZART-4 model to generate the initial condition of the next window. In order to reduce the computational cost and the representative error of XCO<sub>2</sub>, a “super-observation” approach is also adopted, in which a super observation is generated by averaging all observations located within the same model grid (1° × 1°) within a DA window. In addition, to reduce the impact of spurious correlations, a localization technique is employed to determine which super-observations are used for the current grid's optimization. This is based on the correlation coefficient between the flux change of a certain grid and the concentration change at each observation point, and on the space distances between the grid and the observation point. For additional information regarding the “super-observation” approach and the localization technique, please refer to Jiang et al. (2021).

In the system, both the biosphere and ocean fluxes are optimized, and others are prescribed. The prior biosphere flux is simulated using the Boreal Ecosystem Productivity Simulator model (J. M. Chen et al., 1999, 2019; Ju et al., 2006), which is driven by remotely sensed global leaf area index (LAI) (Y. Liu et al., 2012) and clumping index (L. He et al., 2012). Fossil fuel, fire, and prior ocean CO<sub>2</sub> fluxes are obtained from CarbonTracker 2019B (Peters et al., 2007), with updates documented at <http://carbontracker.noaa.gov>. In CT2019B, the “Miller” and ODIAC emissions datasets were used for fossil fuel CO<sub>2</sub> emissions; two models are used to provide prior estimates of air-sea CO<sub>2</sub> flux, the Ocean Inversion Fluxes scheme and an updated version of the Takahashi et al. (2009) pCO<sub>2</sub> climatology. Fire CO<sub>2</sub> emission is obtained from the Global Fire Emissions Database, Version 4.1 (GFED4.1s, van der Werf et al., 2017). Since CT2019B only provides prior data till the March of 2019, the fossil fuel emission is adjusted from the emission in 2018 by ratios of 2019/2018 in different countries or regions that are calculated based on the 2018 and 2019 emissions compiled by the Global Carbon Budget 2020 (Friedlingstein et al., 2020). The ocean flux in 2019 is assumed to be the same as in 2018. The output from the GCAS v2 system with the assimilation of GOSAT XCO<sub>2</sub> retrievals has been used to estimate regional carbon budgets (W. He, Jiang, Wu, et al., 2022; Jiang et al., 2021; Jiang, He, et al., 2022; Jiang, Ju, et al., 2022). Here we estimate global carbon fluxes using only the OCO-2 column-averaged dry-air mole fraction (XCO<sub>2</sub>) retrievals (ACOS XCO<sub>2</sub> v10) (O'Dell et al., 2018). For this study, only the land retrievals (Land Nadir + Land Glint, LNLG) were assimilated. Before being used in the inversion system, the pixel-level XCO<sub>2</sub> data were filtered with `xco2_quality_flag`, and then re-gridded to a spatial resolution of 1° × 1° (Jiang, Ju, et al., 2022).

The carbon flux derived with GCAS v2 had been validated before when assimilating GOSAT XCO<sub>2</sub> retrievals (W. He, Jiang, Wu, et al., 2022; Jiang et al., 2021; Jiang, He, et al., 2022; Jiang, Ju, et al., 2022). Here extra validation and evaluation work was conducted for moving to assimilate OCO-2 XCO<sub>2</sub> retrievals. We evaluated the OCO-2 inversion using 70 surface CO<sub>2</sub> sites from the ObsPac GLOBALVIEWplus v7.0 data product (Masarie et al., 2014) over the globe (Table S1 and Figure S1 in Supporting Information S1 shows the evaluation over East Asia) and aircraft data from the Comprehensive Observation Network for Trace gases by AirLiner project (CONTRAIL, Machida et al., 2008) over East Asia (Figure S2 in Supporting Information S1). The results suggest the GCAS OCO-2 inversion imposed robust constraints on regional flux estimates.

### 2.2. CAMS CO<sub>2</sub> Inversions

In the CAMS CO<sub>2</sub> inversion system, atmospheric transport is simulated using the general circulation model of the Laboratoire de Meteorologie Dynamique (LMDz) that is driven by ERA5 meteorological fields, the prior

CO<sub>2</sub> surface fluxes are from a climatology of natural land fluxes simulated by the ORCHIDEE model. The inversion relies on a variational formulation of Bayes theory. CAMS CO<sub>2</sub> inversions consist of both OCO-2 XCO<sub>2</sub> (Chevallier et al., 2019) and surface CO<sub>2</sub> based inversions (Chevallier et al., 2010). In this study, both versions are used for our analyses. We use monthly averaged net land-atmosphere fluxes of CO<sub>2</sub> at a spatial resolution of 1.875° (latitude) × 3.75° (longitude). The OCO-2 inversion (version FT21r2) spans over 2015–2021 using version 10r of NASA's OCO-2 XCO<sub>2</sub> retrievals, and the in situ inversion (version v20r2) spans over 1979–2020 using surface CO<sub>2</sub> observations. The estimated fluxes from CAMS OCO-2 inversions have been successfully applied in a couple of studies (Kwon et al., 2021; K. Wang et al., 2021). It is worth mentioning that the CAMS OCO-2 inversion had also participated in the OCO-2 MIP (OCO-2 MIP), in which it strictly follows the project protocols, which are different from the CAMS operational procedure in terms of observation error and prior fossil fuel fluxes. In the operational procedure, the gridded data set of monthly fossil fuel emissions (GCP-GridFED version 2020.1 (Jones et al., 2021)) was used.

### 2.3. OCO-2 Model Inter-Comparison Project

The Orbiting Carbon Observatory-2 (OCO-2) MIP is a collaborative effort among atmospheric CO<sub>2</sub> modelers to study the impact of assimilating OCO-2 retrieval data into atmospheric inversion models. In this study, we employed the carbon fluxes from both v9 (Crowell et al., 2019; Peiro et al., 2022) and v10 inversions (Byrne et al., 2023), which used NASA's operational bias-corrected OCO-2 L2 Lite XCO<sub>2</sub> product v9r and v10r retrievals, respectively ((Kiel et al., 2019), <https://daac.gsfc.nasa.gov>). The v9 MIP includes 10 inversion models, including Ames, Baker, CAMS, CMS-Flux, CSU, CT, LoFi, OU, TM5-4DVAR, and UT, while The v10 MIP includes all v9 participated models plus four extra models, that is, COLA, JHU, NIES, and WOMBAT. All these models were run following a unified protocol that required them to use the same input of assimilated OCO-2 XCO<sub>2</sub> data, data uncertainties, and anthropogenic emissions (e.g., for v10 the ODIAC 2020 was used). However, the LoFi inversion adopts a different method (low-order) from general flux inversion systems for the flux estimate and it was excluded from the model ensemble calculation of the OCO-2 MIPs. The outputs of the two MIPs cover the time periods 2015–2018 and 2015–2020, respectively. Detailed information about these models is shown in Table 1. The estimated fluxes from this intercomparison project have been thoroughly verified and analyzed for continental carbon budgets worldwide (Crowell et al., 2019; Peiro et al., 2022). The MIP includes different inversion experiments assimilating various types of observational constraints. In this study, we used the “LNLG” version that assimilated both OCO-2 Land Nadir and Land Glint retrievals, and the “IS” version that assimilated surface in situ CO<sub>2</sub> data, which was also employed for comparative analyses.

### 2.4. Global Operational Atmospheric Inversion Systems Assimilating In Situ CO<sub>2</sub> Data

In addition to the in situ CO<sub>2</sub> based global inversions (IS) from CAMS and OCO-2 MIPs, we also used carbon flux estimates from CarbonTracker Europe (CTE2020) (Peters et al., 2010; van der Laan-Luijkx et al., 2017), CarbonTracker (CT2019B) (Jacobson et al., 2020; Peters et al., 2007), and Jena CarboScope (Rödenbeck et al., 2003, 2018) for comparison. The CTE system (Peters et al., 2010; van der Laan-Luijkx et al., 2017) developed at Wageningen University (<http://www.carbontracker.eu>) assimilates global air samples of CO<sub>2</sub> mole fractions to adjust prior surface carbon fluxes simulated by the SiBCASA model. For this study, we used the monthly CTE2020 fluxes with a spatial resolution of 1° × 1°. The CT system (Peters et al., 2005, 2007), was developed at the National Oceanic and Atmospheric Administration of the U.S. (CarbonTracker CT2019B, <http://carbon-tracker.noaa.gov>). We used the monthly CT2019B fluxes at a spatial resolution of 1° × 1°. The Jena CarboScope product was developed at Max Planck Institute for Biogeochemistry in Jena (MPI-BGC, <http://www.bgc-jena.mpg.de/CarboScope/>), which provides global monthly fluxes at a spatial resolution of 2.75° × 2°. The Jena CarboScope s10 v2020 inversion covers the period 2010–2019, which assimilates surface CO<sub>2</sub> observations from 75 stations (more than previous versions) over the globe.

### 2.5. Bottom-Up Estimates From Terrestrial Biosphere Models

We also compare our estimate with the output of an ensemble of state-of-the-art process-based models from the TRENDY project (version 9) (Sitch et al., 2015). We employed 12 models, namely CABLE-POP (Haverd et al., 2018), CLASSIC (Melton et al., 2020), IBIS (Foley et al., 1996), ISAM (Jain et al., 2013), ISBA-CTRIP

**Table 1**  
*Configuration of Each Simulation Used in the Model Inter-Comparison Project Comparison*

Model	Institution	Transport model	Meteorology	Meteorology resolution (degree)	Prior biosphere flux	Inverse method	References
AMES	NASA Ames	GEOS-Chem	MERRA2	4° × 5°	CASA- GFED4.1s	4D-Var	Philip et al. (2019, 2022)
Baker	CSU	PCTM	MERRA2	1° × 1.25° prior, 4° × 5° opt	CASA- GFED3	4D-Var	Baker et al. (2006, 2010)
CAMS	LSCE	LMDz	ERA-Interim (for v9)/ ERA5 (for v10)	1.9° × 2.75°	ORCHIDEE	Variational	Chevallier et al. (2005, 2019)
CMS-Flux	NASA JPL	GEOS-Chem	GEOS-FP	4° × 5°	CARDAMOM	4D-Var	J. Liu et al. (2021) and R. Liu et al. (2021)
COLA <sup>a</sup>	IAPCAS	GEOS-Chem	MERRA2	4° × 5°	VEGAS	EnKF	Z. Liu et al. (2022)
CSU	CSU	GEOS-Chem	MERRA2	4° × 5°	SiB4	Bayesian synthesis	Schuh et al. (2013)
CT	NOAA	TM5	ERA-Interim	2° × 3°/1° × 1°	CASA GFED4.1s	EnKF	Jacobson et al. (2020)
JHU <sup>a</sup>	JHU	PCTM	MERRA2	4° × 5°	CASA GFED4.1s	GIM	Z. Chen, Huntzinger, et al. (2021) and Miller et al. (2020)
LoFi	NASA	TM5	GEOS5	0.5° × 0.625°	CASA-GFED3	N/A	Z. Chen, Liu, et al. (2021) and Weir et al. (2021)
NIES <sup>a</sup>	NIES	NIES-TM/FLEXPART	JRA-25	3.75° × 3.75°/1° × 1°	VISIT	4D-Var	Maksyutov et al. (2021)
OU	U. Oklahoma	TM5	ERA-Interim	4° × 6°	CASA-GFED3	4D-Var	Crowell et al. (2019)
TM5-4DVAR	U. Maryland	TM5	ERA-Interim	2° × 3°	SiBCASA	4D-Var	Basu et al. (2013, 2018)
UT	U. Toronto	GEOS-Chem	MERRA2	4° × 5°	BEPS	4D-Var	Deng et al. (2014, 2016)
WOMBAT <sup>a</sup>	U. Wollongong	GEOS-Chem	MERRA-2	2° × 2.5°	SiB4	Synthesis with MCMC	Zammit-Mangion et al. (2022)

<sup>a</sup>The newly added inversion models in the v10 MIP. The official websites for v9 and v10 MIPs are [https://www.gml.noaa.gov/ccgg/OCO2\\_v9mip/](https://www.gml.noaa.gov/ccgg/OCO2_v9mip/) and [https://www.gml.noaa.gov/ccgg/OCO2\\_v10mip/](https://www.gml.noaa.gov/ccgg/OCO2_v10mip/), respectively.

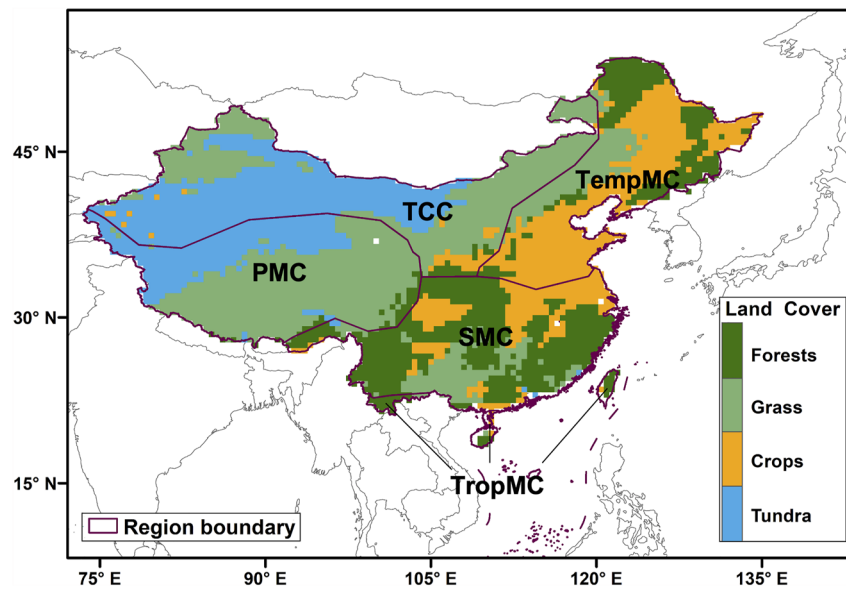


**Figure 1.** (a) Climate zones and (b) ecoregions over China. TropMC—tropical monsoon climate; SMC—subtropical monsoon climate; PMC—plateau mountain climate; TCC—temperate continental climate; and TempMC—temperate monsoon climate.

(Delire et al., 2020), LPJ (Poulter et al., 2011), LPX-Bern (Lienert & Joos, 2018), OCN (Zaehle & Friend, 2010), ORCHIDEE (Krinner et al., 2005), ORCHIDEE-CNP (Y. Sun et al., 2021), ORCHIDEEv3 (Vuichard et al., 2019), and YIBs (Yue & Unger, 2015). For the comparison, we used simulations under scenario S3, which considered impacts from CO<sub>2</sub>, climate, land use, and gridded atmospheric nitrogen deposition and nitrogen fertilizers. These simulations were conducted using the merged monthly Climate Research Unit and 6-hourly Japanese 55-year Reanalysis (JRA-55) data set, and they provide monthly fluxes at a spatial resolution of 0.5° × 0.5°.

## 2.6. Ancillary Data Sets

To evaluate the seasonality of inverted net biome production (NBP) derived from OCO-2 XCO<sub>2</sub>, we included two ancillary variables, LAI and SIF, retrieved from satellite observations. These variables can reasonably capture the seasonal variations of vegetation growth and in principle have some levels of agreement with the seasonal cycles of GPP and NBP. GLOBMAP LAI (v3) provides a consistent long-term global LAI product (1981–2020) at a gridded 8 km resolution by quantitative fusion of Moderate Resolution Imaging Spectroradiometer (MODIS) and historical Advanced Very High Resolution Radiometer data (Y. Liu et al., 2012). In addition, remotely sensed SIF has shown great promise for probing spatiotemporal variations of GPP (Guanter et al., 2014; Li et al., 2018). Here we use a reconstructed contiguous SIF data set over 2000–2020 (Y. Zhang et al., 2018) based on OCO-2 data and MODIS data (named CSIF, v2). We aggregate the data into monthly time steps.

We used the Global Land-surface Evaporation Amsterdam Methodology (GLEAM, version 3.5a) surface soil moisture (SM) data to indicate drought stress. The GLEAM SM was derived from a combination of both passive and active sensors based satellite surface SM products through DA (Martens et al., 2017; Miralles et al., 2011). It is provided at a daily scale over 1980–2020 with a spatial resolution of 0.25° × 0.25°. In addition, SIF and LAI were used to indicate drought impacts on the terrestrial ecosystems.

## 2.7. Climate Zones and Ecoregions

The five main climate zones and four aggregated ecoregions over China are shown in Figure 1. These climate zones include tropical monsoon climate (TropMC), subtropical monsoon climate (SMC), plateau mountain climate (PMC), temperate continental climate (TCC), and temperate monsoon climate (TempMC). The ecoregions were aggregated based on the IGBP classification scheme of MODIS land cover data (MCD12C1) for the year 2012 at a spatial resolution of 1° × 1°. Due to the relatively small area of the TropMC zone, it was combined with the SMC zone in our analysis, and referred to as “Trop-SMC.”

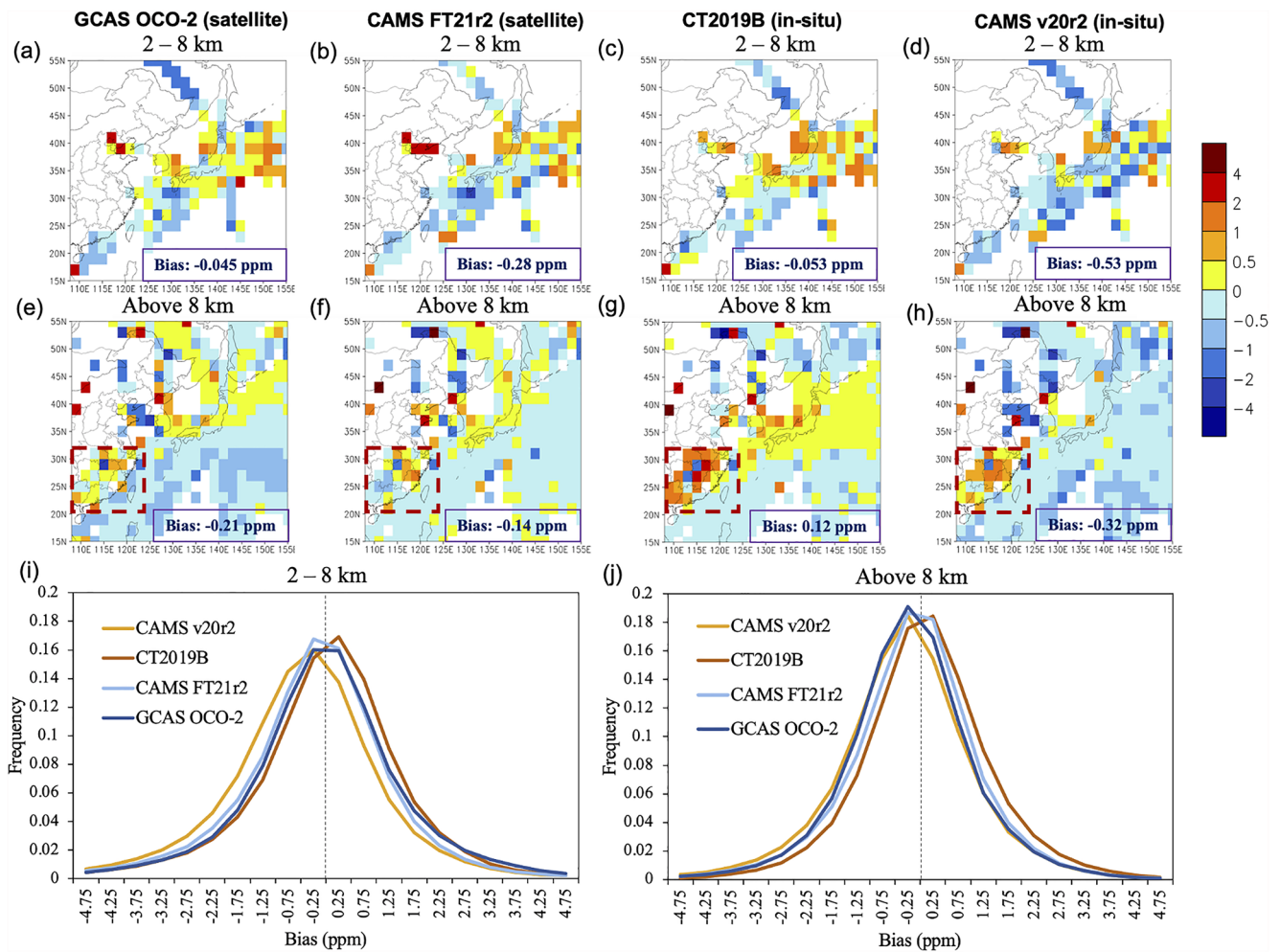


**Figure 2.** Comparison of the biases between optimized mole fractions by the in situ or satellite inversions and Comprehensive Observation Network for Trace gases by AirLiner project aircraft observations during 2015–2019 over one part of East Asia (15°–55°N, 108°–155°E). The simulations at two elevation levels, 2–8 and above 8 km, were evaluated. The boundary layer below 2 km was not included in the assessment, since this level is affected by high emissions from airports. The elevation level of 2–8 km represents the height for aircraft takeoff and landing, while above 8 km corresponds to normal flight. Compared with these in situ inversions, the biases for Orbiting Carbon Observatory 2 inversions were clearly lower in southeastern China (indicated in red rectangles).

### 3. Results

#### 3.1. Improved Posterior CO<sub>2</sub> Simulation by OCO-2 Inversions Compared to In Situ Inversions: Evaluated With CONTRAIL Aircraft Observations

To evaluate and compare the performance of OCO-2 inversions and in situ inversions on flux estimates, we investigated the biases between optimized mole fractions by either in situ or satellite inversions and CONTRAIL aircraft observations during 2015–2019 in East Asia (15°–55°N, 108°–155°E; Figure 2). We evaluated two elevation levels, 2–8 km and above 8 km. The boundary layer below 2 km, which is affected by high emissions from airports, was not included in the assessment. The elevation level of 2–8 km represents the height for aircraft takeoff and landing, while above 8 km corresponds to normal flight, basically corresponding to the middle troposphere and the upper troposphere, respectively. Compared to in situ inversions, OCO-2 inversions generally displayed lower biases at either the 2–8 km (Figures 2a–2d) or above 8 km (Figures 2e–2h) height levels. The exception is CT2019B, which assimilated partial CONTRAIL data, resulting in bias values that were lower than those of both the CAMS in situ inversion at the 2–8 km level and both satellite inversions at the above 8 km level (Figures 2c and 2g). With the same inversion system, the CAMS satellite inversion exhibited substantially lower bias values than the CAMS in situ inversion across the whole region (Figure 2b vs. Figure 2d, Figure 2f vs. Figure 2h). Moreover, in southeastern China, we observed clearly lower biases for the OCO-2 inversions

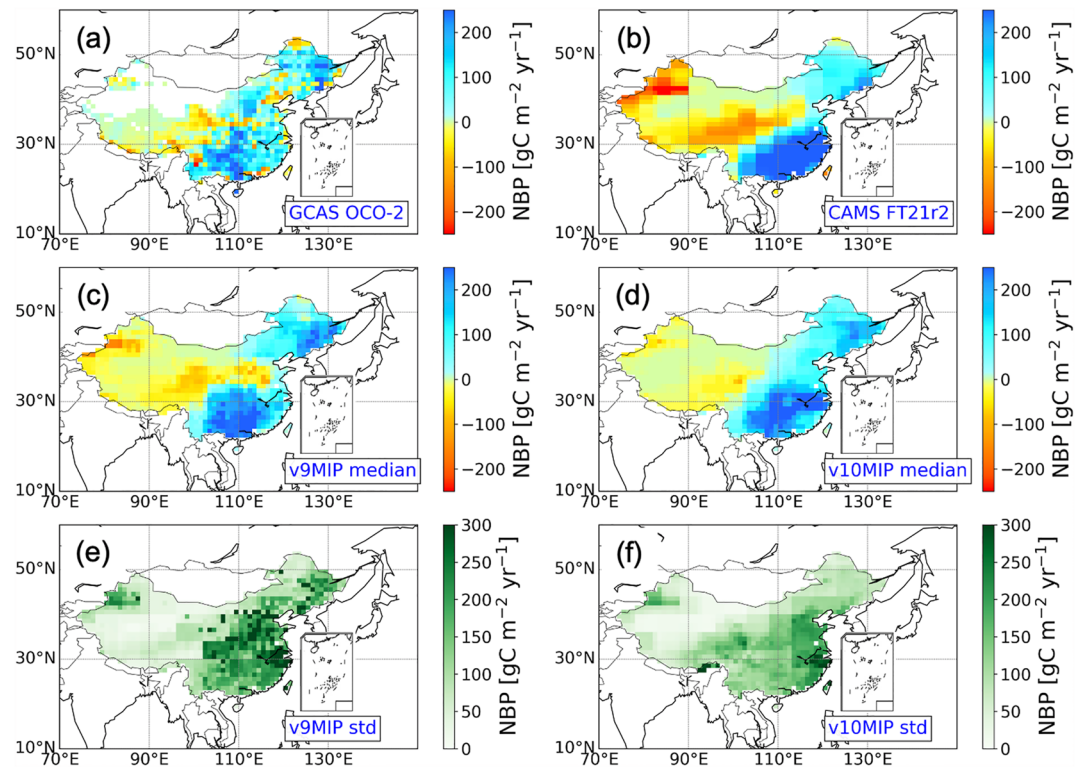


**Figure 3.** Mean annual distribution of China's carbon sink over 2015–2019. Note that in panel (a), the white area in the upper left corner indicates missing values, which originates from the prior flux model setup for a desert area in northwest China.

compared to both in situ inversions at the above 8 km level (Figures 2e–2h). When examining the frequency of biases (Figures 2i and 2j), the OCO-2 inversions exhibit bias values that are more concentrated to zero, while in situ inversions either show larger positive biases or negative biases, especially for the 2–8 km level. These results indicate that OCO-2 XCO<sub>2</sub> retrievals have imposed improved constraints on the regional carbon flux estimate in East Asia.

### 3.2. Spatial Distributions of NBP Across China

We conducted an analysis of the spatial distribution of multi-year mean annual NBP in China over the period 2015–2019 (Figure 3). In general, the different OCO-2 inversions consistently identified the strongest annual carbon sink in the southern region and the second largest sink region in the northeast (Figures 3a–3d). They also indicated that most of the west, especially in the Qianghai-Tibet Plateau and northwest Xinjiang, is a carbon source. The MIP inversions revealed a larger inter-model discrepancy in eastern China than in the other regions, which is reduced substantially in the v10 MIP compared to the v9 MIP (Figures 3e and 3f). In comparison to most in situ CO<sub>2</sub> based inversions (Figure S3 in Supporting Information S1) and biosphere model simulations (Figure S4 in Supporting Information S1), the spatial patterns revealed by the OCO-2 inversions show clear differences. Regionally, the strongest annual carbon sink was found to be in the Trop-SMC and TempMC climate zones (Figure 4a), mainly contributed by forests and crops, respectively (Figure 4b). Most OCO-2 inversions suggested that PMC is a carbon source and TCC could be a small carbon source or carbon neutral (Figure 4a). The tundra ecosystem is likely a carbon source, and the grass ecosystem could be a small carbon source or sink (Figure 4b). Notably, in contrast with the OCO-2 inversions, the majority of in situ CO<sub>2</sub> based inversions and all biosphere model simulations suggest that PMC and TCC are carbon sinks (Figures 4a, 4c, and 4e), and the grass ecosystem acts as important carbon sink (Figures 4b, 4d, and 4f). In addition, compared with the OCO-2 inversions, the in situ inversions estimated much smaller carbon sinks in southern China or the Trop-SMC zone (Figure S3 in Supporting Information S1 vs. Figure 3, and Figure 4c vs. Figure 4a), which coincides with their larger positive biases of CO<sub>2</sub> concentration in southern China (Figures 2e–2h).



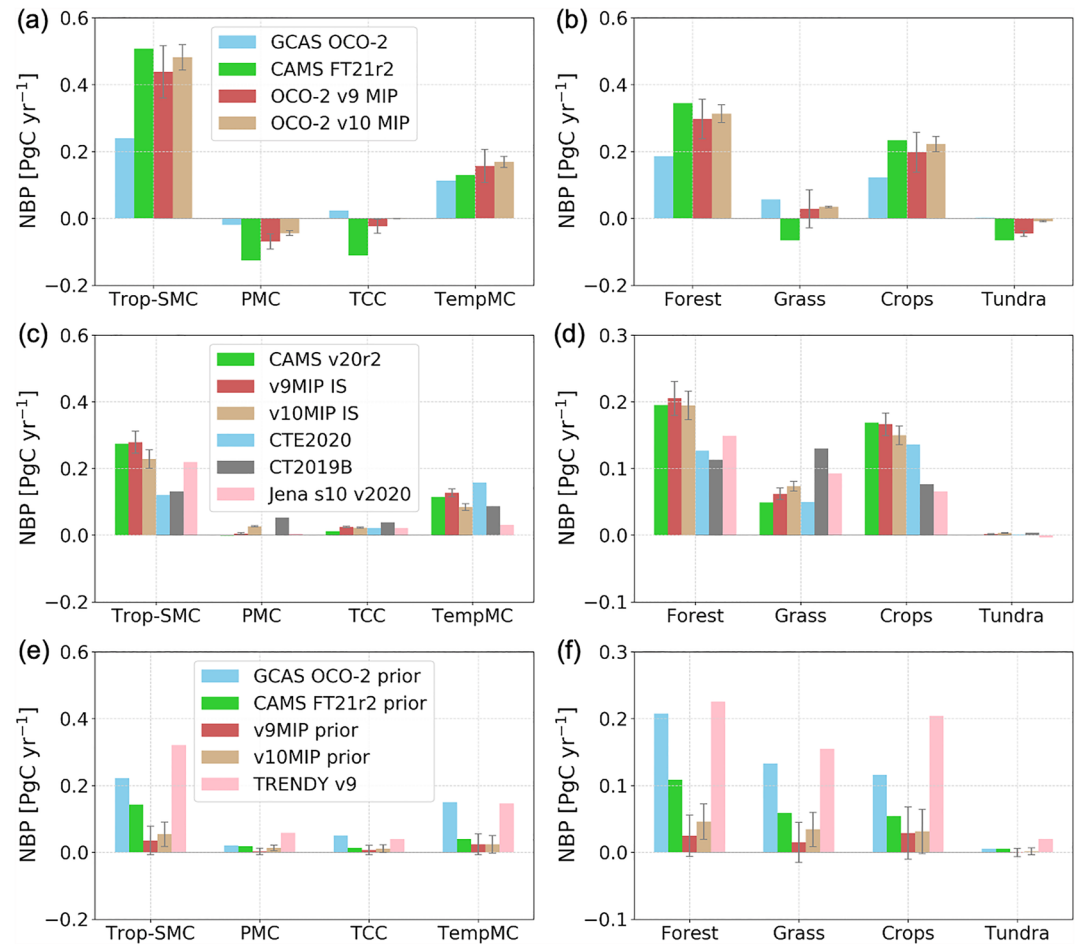


**Figure 4.** The contributions of China's annual carbon sink over 2015–2019 by different climate zones and ecosystems in Orbiting Carbon Observatory 2 inversions (a, b), in situ inversions (c, d), and prior/TBM simulations (e, f). TropMC—tropical monsoon climate; SMC—subtropical monsoon climate; PMC—plateau mountain climate; TCC—temperate continental climate; and TempMC—temperate monsoon climate.

We also analyzed the spatial distribution of peak growing season (July–August) NBP in China averaged over 2015–2019 (Figure 5). The results indicated that the largest carbon sink is in the northeast within the TempMC region, followed by the central region within the Trop-SMC region. This coincides well with China's main agricultural areas in the Northeast Plain, the North China Plain, and the Middle-lower Yangtze Plain (see Figure 1). The Northeast Plain has the largest carbon sink during peak growing seasons, possibly attributed to its fertile black soil that benefits crop productivity. Overall, crops contribute the largest carbon sink, followed by forest and grass ecosystems, which is distinct from the distribution of annual carbon flux. Notably, CAMS FT21r2 and OCO-2 MIPs indicated a clear carbon source in part of the southwest (west Yunnan Province). Furthermore, the east Qianghai-Tibet Plateau is identified as a carbon sink. In MIP inversions, the inter-model discrepancy has been significantly reduced in the v10 MIP compared to the v9 MIP (Figures 5e and 5f), and this discrepancy is much smaller than that observed in the annual distribution (see Figures 3e and 3f). Comparing the spatial distributions of annual and peak growing season NBP, we observed that although most areas are carbon sinks during the peak season, they are not on a yearly basis. It should be noted that the plausible peak growing season NBP spatial patterns are not able to be consistently revealed by either in situ inversions (Figures S5 in Supporting Information S1) or biosphere model simulations (Figure S6 in Supporting Information S1). When aggregating into regions, we found that in the OCO-2 inversions, the TempMC region and crops contribute most significantly to the carbon sink during peak growing seasons as observed in OCO-2 inversions (Figures 6a and 6b). However, such dominance is not easily distinguished in most in situ inversions (Figures 6c and 6d) or biosphere model simulations (Figures 6e and 6f).

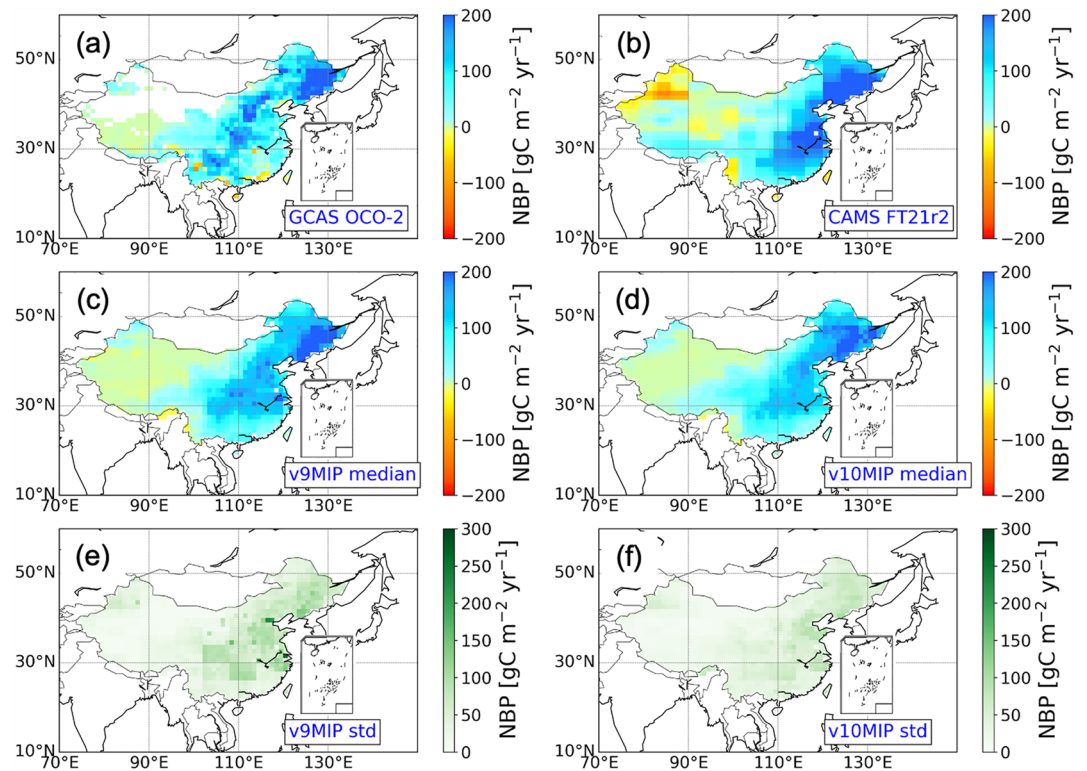


**Figure 5.** Mean peak growing season (July–August) distribution of China's carbon sink over 2015–2019.

### 3.3. Seasonal Cycles of NBP Across Climate Zones and Ecosystems

We analyzed the mean seasonal cycles of NBP estimated by the different OCO-2 inversions over 2015–2019 and compared them with those by in situ inversions and prior/TBM simulations (Figure 7). The seasonal cycles of the different OCO-2 inversions converge well over the entire domain of China (Figure 7a), with the peak carbon sink occurring in July (about  $0.30 \text{ PgC mon}^{-1}$ ). The peak carbon sink is comparable to that of in situ inversions (Figure 7b) but is clearly greater than that of prior/TBM simulations (about  $0.20 \text{ PgC mon}^{-1}$ , Figure 7c). Moreover, the NBP seasonal cycles of the OCO-2 inversions converged clearly better than these of the in situ inversions.

When broken down into climate zones (Figures 8a–8d), the TempMC region on average exhibits the largest peak NBP, with a value close to  $0.15 \text{ PgC mon}^{-1}$ , followed by the Trop-SMC region, at around  $0.10 \text{ PgC mon}^{-1}$ , according to most inversions. In contrast, the PMC region has the smallest peak NBP, which is less than  $0.02 \text{ PgC mon}^{-1}$ . These zones appear to serve as carbon sources in winter and carbon sinks in summer. The Trop-SMC zone has the longest period for carbon uptake (March–October) and a short period for carbon release, starting to act as a carbon sink in the spring, while the PMC region only becomes a carbon sink in the summer. Generally, the South (Trop-SMC) begins behaving as a carbon sink earlier than the North (TCC and TempMC), with the Qinghai-Tibet Plateau (PMC) being the latest. Most regions (Trop-SMC, TCC, and TempMC) reach their peak of carbon sink in July, while the PMC reaches its peak in August. Obviously, the peak carbon flux (carbon uptake) of TempMC is generally larger than that of Trop-SMC. Additionally, among all climate zones, TempMC has the largest negative carbon flux (carbon release). Across different climate zones, the various OCO-2 inversions show good agreement, with the best coinciding results in TempMC and Trop-SMC, which are major carbon sink regions. In comparison, the OCO-2 inversions were more consistent in TempMC, which is less uncertain than other climate zones in the OCO-2 MIPs. Consistency was observed for the results of OCO-2 v9 MIP and OCO-2 v10 MIP over different regions. However, subregional-scale across-model consistencies are generally worse for either in situ inversions (Figure S7 in Supporting Information S1) or biosphere model simulations (Figure S8 in Supporting Information S1).

We also analyzed the mean seasonal cycles of NBP across various ecosystems revealed by the OCO-2 inversions (Figures 8e–8h). The crops and forest ecosystems displayed a clear peak in NBP in July, with grass and tundra

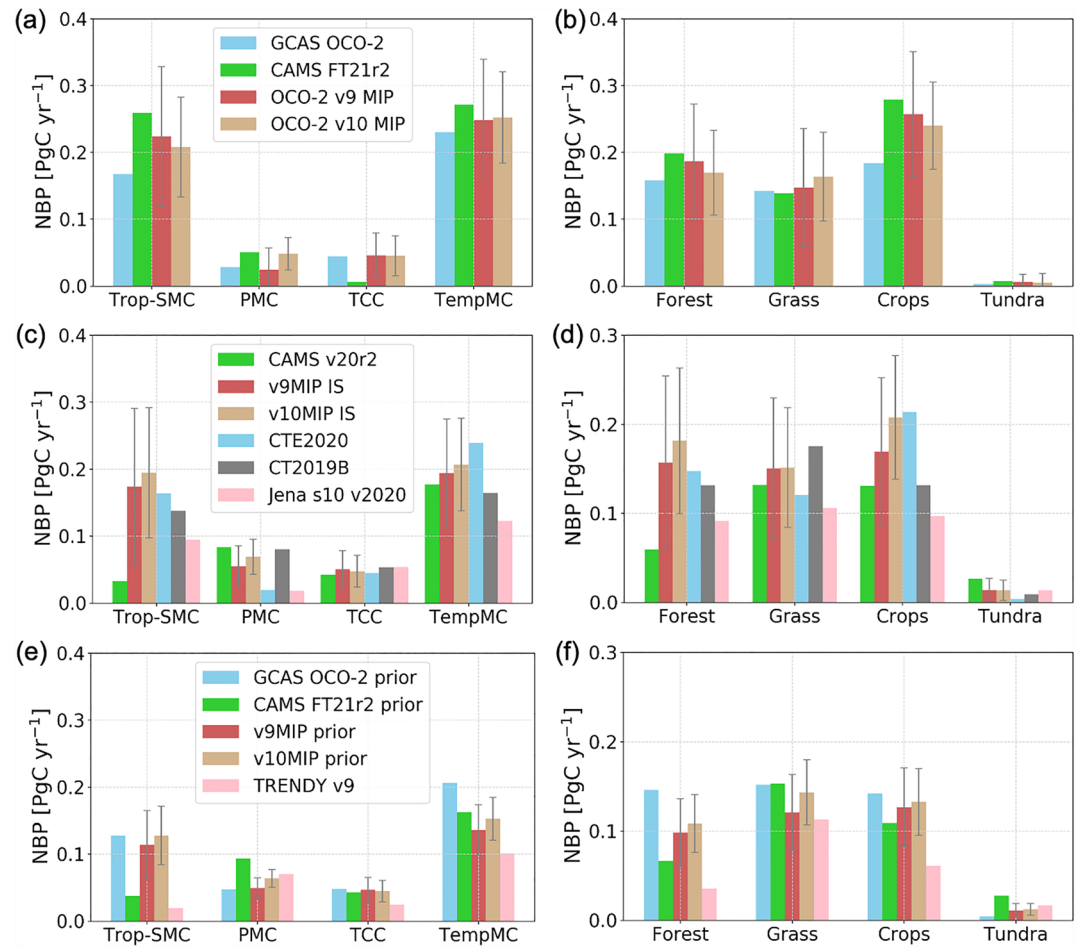


**Figure 6.** The contributions of China's peak growing season (July–August) carbon sink over 2015–2019 by different climate zones and ecosystems in Orbiting Carbon Observatory 2 inversions (a, b), in situ inversions (c, d), and prior/TBM simulations (e, f). TropMC—tropical monsoon climate; SMC—subtropical monsoon climate; PMC—plateau mountain climate; TCC—temperate continental climate; and TempMC—temperate monsoon climate.

ecosystems peaking slightly later, with a broad peak between July and August. The former two ecosystems also exhibited a longer carbon uptake period of more than 5 months, while the latter two have noticeably shorter carbon uptake periods, about 4 months or less. Furthermore, the crop ecosystem displayed the greatest amplitude of the seasonal cycle in NBP, followed by forest, grass, and tundra. Additionally, the grass and the crop ecosystems showed a clearly greater amplitude for carbon release compared to the forest ecosystem during the non-growing season. In contrast, the tundra ecosystem displayed relatively weak carbon sink capacity, serving as a carbon sink only during the summer months, but acting as a carbon source over most of the year, exhibiting a substantially larger amplitude for carbon release during the non-growing season than for carbon uptake during the growing season. The different OCO-2 inversions demonstrated fairly good consistency across the four ecosystems, particularly between v9 MIP and v10 MIP.

The OCO-2 inversions outperformed in situ inversions and biosphere model simulations in terms of inter-model consistency for seasonal cycles at subregional scales, especially in the monsoon climate zones (TempMC and Trop-SMC) and the forest and crops ecosystems (Figures S9 and S10 in Supporting Information S1).

### 3.4. Annual Total NBP and IAV Over 2015–2019

Figure 9 shows the total land NBP of China between 2015 and 2019. The GCAS OCO-2 inversion (0.34 PgC/yr) and CAMS FT21r2 (0.38 PgC/yr) estimates are lower than the ensemble median of both OCO-2 v9 MIP ( $0.57 \pm 0.19$  PgC/yr) and OCO-2 v10 MIP ( $0.47 \pm 0.16$  PgC/yr). While the IAVs reflected by different atmospheric

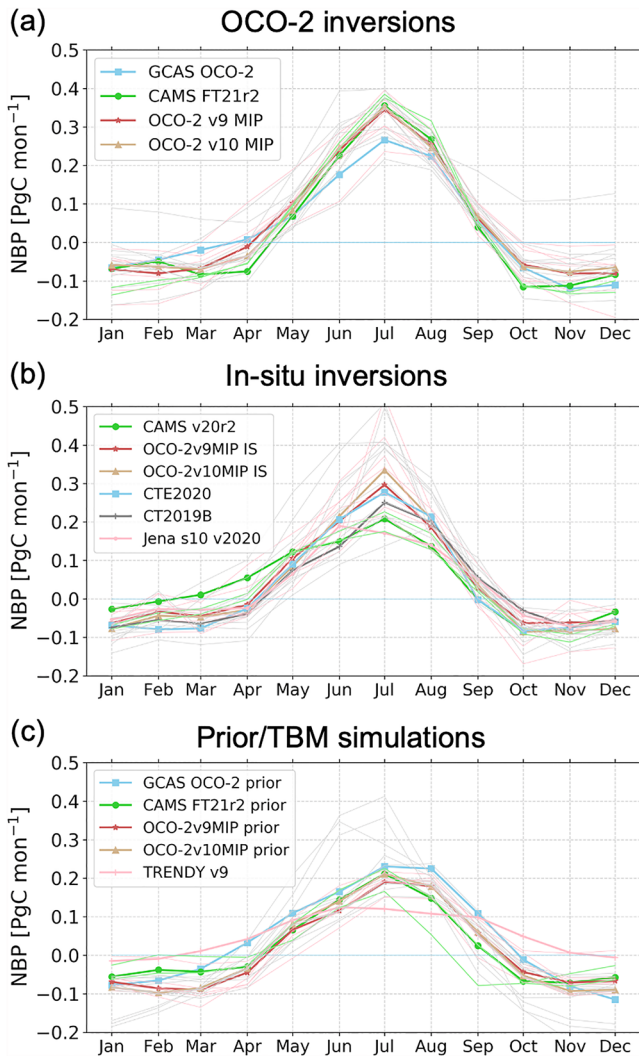


**Figure 7.** Multi-year mean seasonal cycles of net biome production for China over 2015–2019 estimated by (a) Orbiting Carbon Observatory 2 inversions, (b) in situ inversions, and (c) prior/TBM simulations. The thin lines in pink and gray indicate individual v9 and v10 Model Inter-comparison Project inversions, respectively. The light green lines mark Copernicus Atmosphere Monitoring Service inversions in the two Model Inter-comparison Projects.

inversions were not exactly consistent with each other, they consistently pointed to the weakest carbon uptake occurring in 2019 (Figure 9a). Most individual inversions of the v10 MIP also revealed this carbon sink reduction (Figure S11 in Supporting Information S1). This reduction is likely associated with SM droughts that occurred in North China, the southwest, and eastern China along the basin downstream of Yangtze River (Figure S12 in Supporting Information S1). However, the estimated NBP by most in situ inversions (Figure 9b) and prior/TBM simulations (Figure 9c) did not respond to the 2019 drought.

Notable reductions in TCC and TempMC were seen in monthly carbon sink anomalies across climate zones for 2019, and in PMC and TCC for 2015 and 2016 (Figure 10), which may be attributed to the impact of the 2015/2016 El Niño event. Unlike the 2019 event, which caused noticeable NBP reductions in almost all climate zones, the 2015/2016 El Niño event induced both reductions (e.g., PMC and TCC) and enhancements (e.g., in Trop-SMC and TempMC) in NBP, largely offsetting each other and resulting in a near-neutral effect on the total carbon sink in China. These divergent NBP variations may be associated with the changed SM status resulting from the 2015/2016 El Niño event, where PMC and TCC became drier while Trop-SMC and TempMC became wetter (Figure S12 in Supporting Information S1). By breaking down into ecosystems (Figure S13 in Supporting Information S1), we found that the 2015/2016 El Niño event only caused a pronounced NBP reduction in the grass ecosystem, while periodical NBP increases were found in the forest and crop ecosystems. During the 2019 drought, the reductions in annual NBP were mainly contributed by the crop and grass ecosystems, which are usually the most drought-vulnerable ecosystems (W. He et al., 2018a). Notably, the substantial NBP anomalies in the TempMC and TCC climate zones that were dominated by crops and grass, respectively, coincided reasonably well with the location of the drought in 2019 (see Figure 11). This drought also caused NBP anomalies in southern China (Trop-SMC), which can be explained as either the inhibited vegetation biochemical or biophysical activities (Figures 11e and 11f). Moreover, it should be noted that considerable uncertainties exist in these OCO-2 inversions for both the multi-year mean NBP and its IAV of China in the period of 2015–2019.

## 4. Discussion

### 4.1. The Size, Spatial Distribution, and Ecosystem Contribution of China's Carbon Sink

The size of China's carbon sink remains a topic of ongoing debate. J. Wang et al. (2020) estimated a large Chinese carbon sink of  $1.11 \pm 0.38$  PgC/yr over 2010–2016 using in situ  $\text{CO}_2$  observations, which was later questioned by Y. Wang et al. (2022) due to the major impact of one particular surface site: they provided a revised estimate at 0.39 PgC/yr after excluding that site. Also, Schuh et al. (2022) pointed out a possible bias due to underestimated vertical mixing in certain atmospheric transport models (GEOS-Chem vs. TM5) over China. Our previous study (W. He, Jiang, Wu, et al., 2022) also investigated this issue and found that the estimate by J. Wang et al. (2020) largely diverged from other estimates by model simulations and atmospheric inversions, presenting an estimate between 0.34 and 0.43 PgC/yr constrained by GOSAT  $\text{XCO}_2$  and land surface variables. In this study, constrained by OCO-2  $\text{XCO}_2$  observations, we estimate a carbon sink of 0.34 PgC/yr over 2015–2019 by the GCAS OCO-2 inversion, while the OCO-2 v10 MIP estimates a stronger carbon sink (about  $0.47 \pm 0.16$  PgC/yr, median  $\pm$  std.). These estimates for the size of China's carbon sink are comparable with the in situ  $\text{CO}_2$  based estimates (Table S2 in Supporting

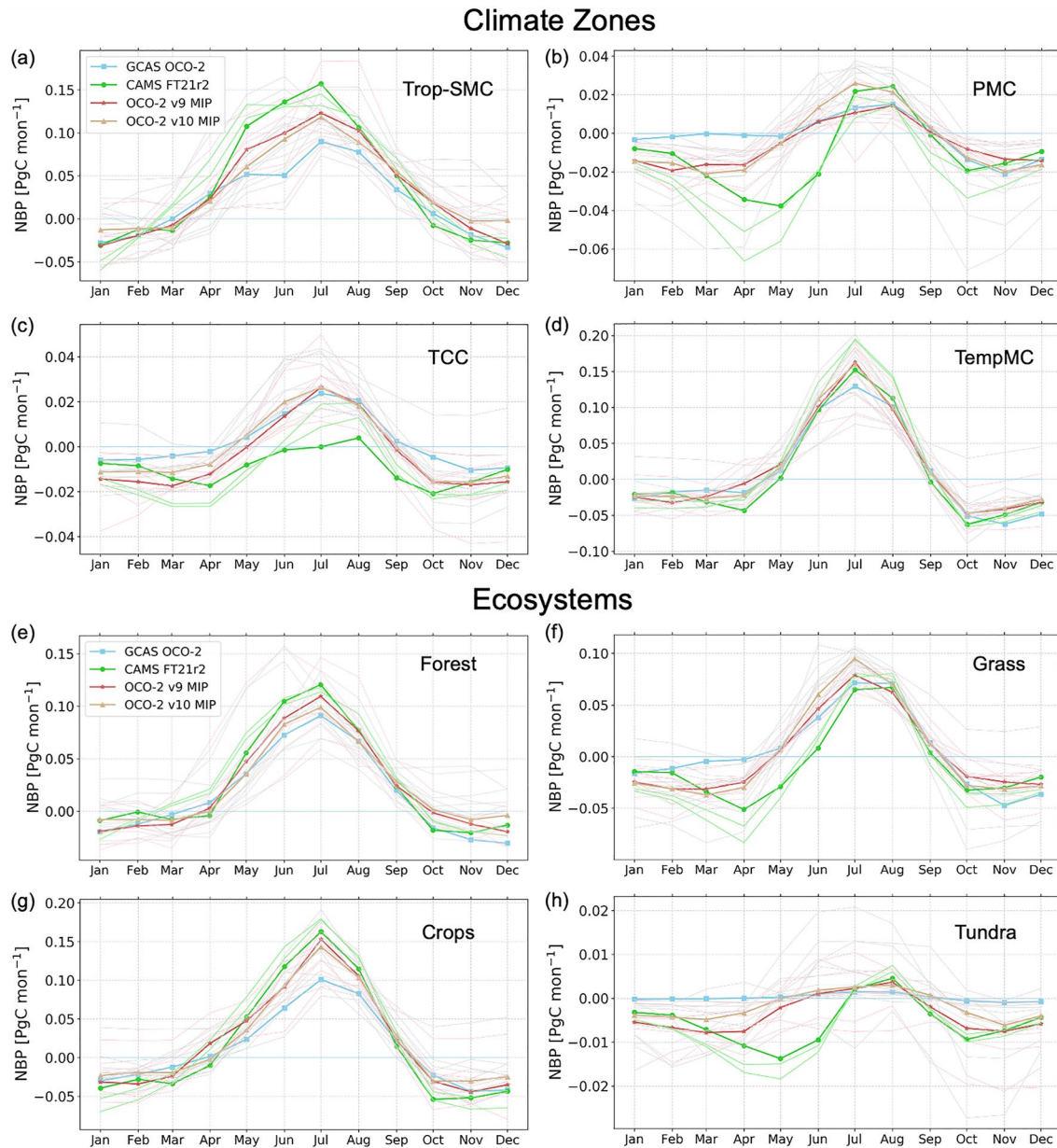


**Figure 8.** Multi-year mean seasonal cycles of net biome production for different climate zones and ecosystems of China over the period 2015–2019. The thin lines in pink and gray indicate individual v9 and v10 Model Inter-comparison Project inversions, respectively. The light green lines mark Copernicus Atmosphere Monitoring Service inversions in the two Model Inter-comparison Projects.

Information S1) and, but are clearly higher than most priors and lower than the ensemble mean of the TRENDY models (Table S3 in Supporting Information S1).

Although considerable uncertainties exist in the size of China's land carbon sink, the spatial distributions inferred by different inversions converge relatively well. For a long time, there was no consensus regarding the spatial distribution of China's carbon sink, with some studies suggesting the largest carbon sink was located in the southeast of China (Tian, Melillo, et al., 2011; Tian, Xu, et al., 2011), while some others suggested the southwest had the largest carbon sink (J. Wang et al., 2020; Ye & Chuai, 2022). However, the various OCO-2 inversions employed in this study suggest the largest carbon sink is present in southern China. This finding is consistent with estimates made by Piao et al. (2009), Yu et al. (2014), Yao et al. (2018), and our previous estimates constrained by either GOSAT XCO<sub>2</sub> or land surface variables plus in situ CO<sub>2</sub> observations (W. He, Jiang, Wu, et al., 2022).

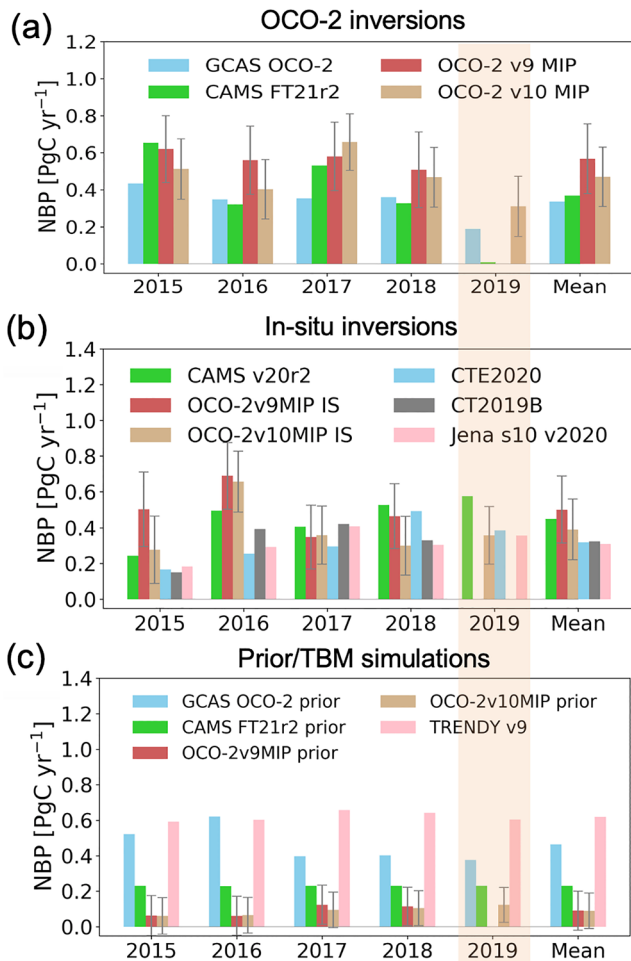


**Figure 9.** Annual net biome production of China over 2015–2019 estimated by (a) Orbiting Carbon Observatory 2 inversions, (b) in situ inversions, and (c) and prior/TBM simulations. The error bar indicates one standard deviation. Note that the Copernicus Atmosphere Monitoring Service prior doesn't contain interannual variability.

Our study further demonstrates that during the peak growing season, the largest NBP occurs in the northeast followed by the other main agricultural areas, which is in agreement with the distribution of China's main crop planting areas. This pattern is similar to that observed in the U.S., where the largest peak growing season carbon uptake takes place in the Corn-Belt agricultural area (Guanter et al., 2014; W. He et al., 2018b, 2021; Hilton et al., 2017; Peters et al., 2007; Schuh et al., 2013; W. Sun et al., 2021).

In terms of ecosystem contribution, our study suggests China's terrestrial carbon sink is mainly contributed by forests and crops, while other ecosystem types act as carbon sources on an annual basis. Our estimates agree with most previous estimates on the large contribution of the forest ecosystem, but present a clearly lower proportion (on average 61.35%) than the 80% reported by Fang et al. (2018) based on a field survey. We estimate a higher contribution by crops (on average 45.23%), while Fang et al. (2018) reported only 12%. This discrepancy in crops originates from methodological differences between the estimates: a bottom-up soil organic carbon inventory by Fang et al. (2018) and top-down atmospheric inversions by this study. The inversions do not reflect carbon lateral transport from the crop area to other regions due to food trade, which represents a gross carbon sink for crops. The roles of grass and tundra as a carbon sink or source are still up for debate (Yang et al., 2022). We estimate the tundra ecosystem as a weak carbon source, whereas Fang et al. (2018) estimated it as a carbon sink, contributing to about 8% of total China's terrestrial carbon sink. A number of eddy flux observation studies have reported persistent carbon emissions in thawing permafrost regions of the tundra over many years (Celis et al., 2017; Schuur et al., 2021), where the tundra ecosystem was mainly distributed. In addition, Fang et al. (2018) reported that the grassland ecosystem is basically a carbon neutral or weak carbon source during the period 2001–2010, which is in line with our estimate. In this regard, more observations are needed for a better understanding of the carbon function of the tundra ecosystem in China.

#### 4.2. Improvements in the Understanding of China's Land Carbon Sink Over In Situ CO<sub>2</sub> Inversions and Biosphere Model Simulations

The OCO-2 XCO<sub>2</sub> inversions show certain improvements over the in situ CO<sub>2</sub> inversions and biosphere model simulations in China's land carbon sink estimation, including improved spatial distributions and seasonal cycles and more plausible IAV.

First, different OCO-2 inversions agree well with each other on the spatial pattern of annual and peak growing season NBP, while in situ CO<sub>2</sub> based inversions (Figures S3 and S5 in Supporting Information S1) and biosphere model simulations (Figures S4 and S6 in Supporting Information S1) do not. The OCO-2 inversions are also much more consistent across different climate zones and ecosystems (see Figures 4 and 6). In terms of annual total carbon fluxes, in contrast to the OCO-2 inversions, the in situ inversions do not consistently show a larger carbon sink in Trop-SMC than in TempMC and only one of the six inversions indicates a carbon source in PMC. Furthermore, the tundra and grass show a carbon source in the OCO-2 inversions while not in either the in situ inversions or the prior/TBMs simulations. During peak growing season, the in situ inversions and the prior/TBMs simulations indicate similar patterns to the OCO-2 inversions, both showing the largest NBP in Trop-SMC and the second largest in TempMC, despite considerable discrepancies among the various estimates. Consistent with the OCO-2 inversions, most in situ inversions also reveal a carbon source in part of the southwest (west Yunnan Province). One clear difference is CAMS v20r2, which reveals an unreasonable carbon source in the southeast (see Figure S5 in Supporting Information S1), as seen in its prior stemmed from the ORCHIDEE model and the TRENDY v9 model ensemble (Figure S6 in Supporting Information S1), but is diminished in the OCO-2 inversions. The spatial distributions of the largest annual and peak growing season NBP coincide well with the

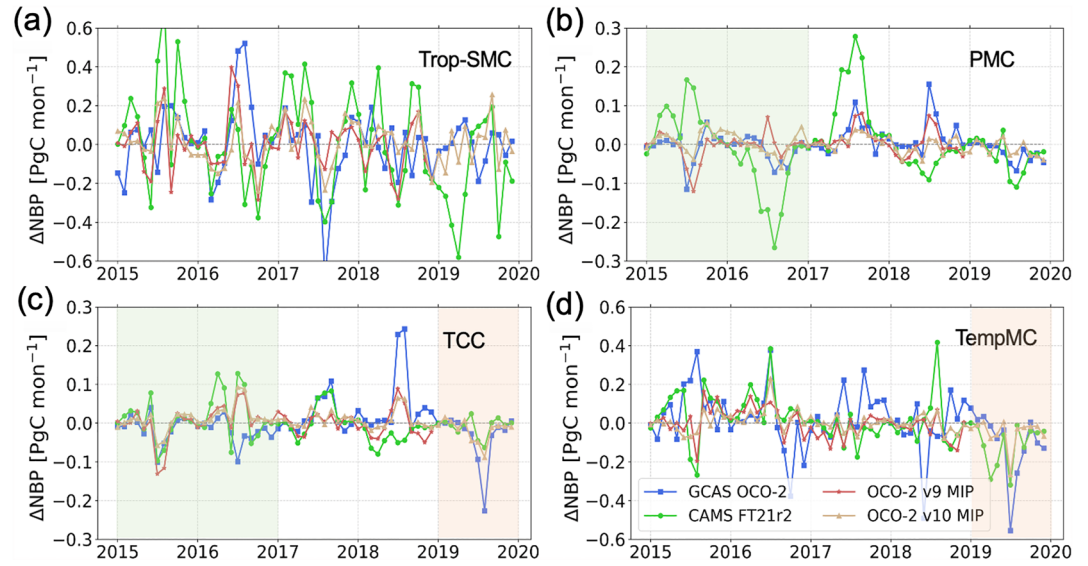


**Figure 10.** Monthly net biome production anomalies of China over 2015–2019 across different climate zones. Note that there is no value for the year 2019 in the v9 Model Inter-comparison Project. The error bar indicates one standard deviation. The shaded areas in shallow green and brown indicate the clear impacts of the 2015/2016 El Niño event and the 2019 drought event, respectively.

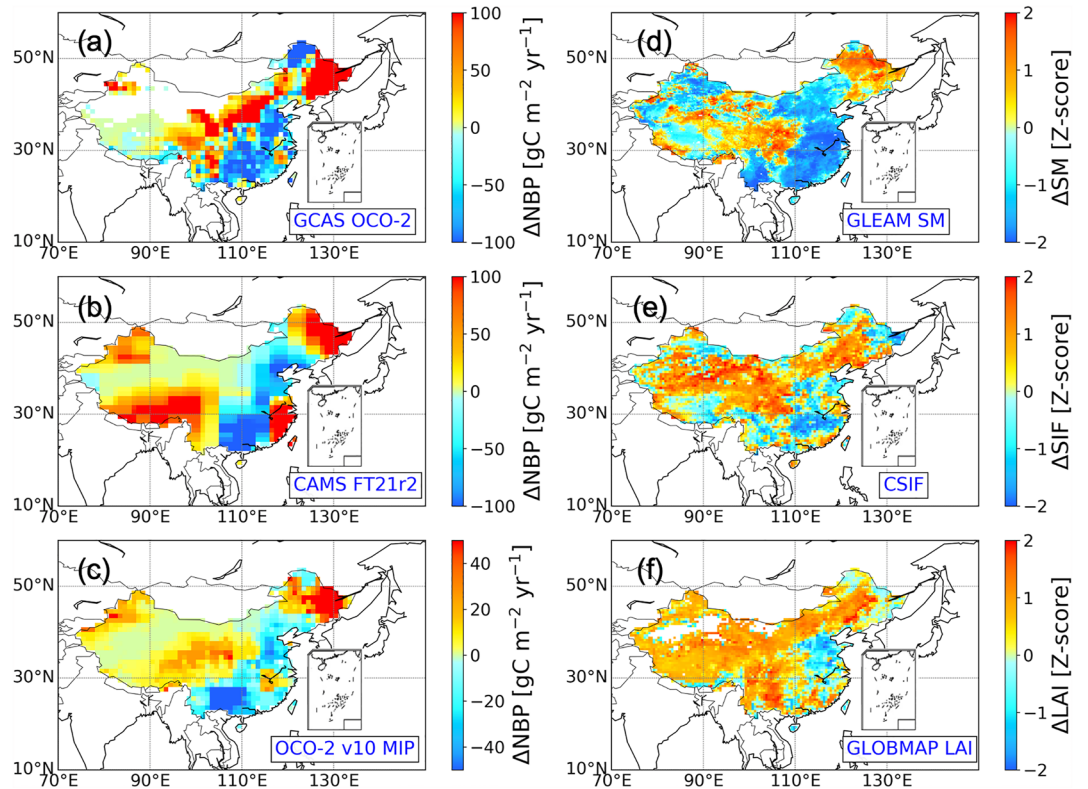


**Figure 11.** Spatial pattern of net biome production anomalies ( $\Delta\text{NBP}$ ) and soil moisture (SM) anomalies ( $\Delta\text{SM}$ ) in the summer-autumn time (June–November) of 2019 estimated by the Orbiting Carbon Observatory 2 (OCO-2) inversions. The anomalies were calculated as the normal values subtracting the multi-year mean values over the study period. The ensemble median of the OCO-2 v10 Model Inter-comparison Project inversions was used. The Z-score of the satellite variables (SM, SIF, and leaf area index) was calculated as  $SV_{Z\text{-score}} = (SV - SV_{\text{mean}}) / SV_{\text{std}}$ , where the mean and std were calculated over the period 2015–2019.

distributions of forest and crops respectively. Interestingly, the OCO-2 inversions have revealed a large carbon source in the Qinghai-Tibet Plateau area, which has not been detected by either the in situ inversion or biosphere model simulations. Because of climate warming, this region experiences enhanced surface carbon uptake while increased carbon emission due to accelerated permafrost degradation and ecosystem respiration. Because the vegetation in this region is less productive, the surface carbon sink is quite limited. In comparison, the carbon emission from accelerated permafrost degradation could be large. Thus, the “seen” large carbon source from OCO-2 is possible. However, because very little CO<sub>2</sub> data in China is available, this emission signal has not been detected by the in situ observations. Regarding TBMs, it is even more difficult for them to accurately simulate the carbon emitted through non-biogenic activity.

Second, in terms of seasonality, compared to the different in situ inversions (Figure 7a, Figure S7 in Supporting Information S1) and prior/TBM simulations (Figure 7b, Figure S8 in Supporting Information S1), clearly improved consistency on the seasonal cycle at sub-regional scales (i.e., over various climate zones) is found with the OCO-2 inversions. For example, the seasonal cycle phase of Trop-SMC and the seasonal cycle amplitude of PMC become more consistent. The TRENDY ensemble estimate appears to have an obviously flatter seasonal variation (Figure 7b) and distinct seasonal cycle phases from other models at subregional scales (e.g., in Trop-SMC and TCC, see Figure S8 in Supporting Information S1) with noticeable double peaks in Trop-SMC. The discrepancies in seasonal cycle phases (e.g., in Trop-SMC, in Figures S7 and S8 in Supporting Information S1) could be explained by the different spatial distributions of the peak growing season NBP (Figures S5 and S6 in Supporting Information S1) in the TRENDY ensemble and the prior of CAMS v20r2 compared to the OCO-2 inversions. In addition, the multi-year mean seasonal cycle of NBP from the OCO-2 inversions correlates highly with that of vegetation variables (SIF and LAI), which is generally higher than in situ inversions and equivalent to or slightly higher than prior simulations by the various inversion systems (Figure S10 in Supporting Information S1). It keeps high correlations at subregional scales while not always for in situ inversions or biosphere model simulations, indicating some improvements in OCO-2 XCO<sub>2</sub> based inversions for recovering the true seasonal cycle of NBP.

Third, the OCO-2 inversions reveal more plausible IAV over the study period. They are able to indicate an annual NBP reduction in 2019 when a severe seasonal drought (Ma et al., 2020) led to SM deficiency (see Figure S12 in Supporting Information S1) and carbon uptake reduction (Figure 11). This NBP reduction was found in most of the OCO-2 v10 MIP individual estimates (Figure S11 in Supporting Information S1). However, we found most in situ inversions (Figure S14 in Supporting Information S1) and prior/TBM simulations (Figure S15 in Supporting Information S1) performed relatively poorly in capturing the impact of the 2019 drought on NBP. The ability of OCO-2 inversions in indicating drought impacts could relate to data coverage. Compared to discrete and sparse in situ CO<sub>2</sub> observations, the satellite XCO<sub>2</sub> observations should be better at capturing spatial details of carbon flux disturbance caused by climate changes. It is very challenging for the current in situ based global inversion systems to capture regional drought impacts due to the very limited in situ CO<sub>2</sub> observations (1–2 sites) having been assimilated (W. He, Jiang, Wu, et al., 2022). Our analyses in this study offer important evidence supporting that OCO-2 inversions have a good capacity in capturing regional drought impact on land carbon sinks, which has also been reported in our recent study about the European droughts (W. He et al., 2023).

### 4.3. Uncertainties in OCO-2 XCO<sub>2</sub> Inversions and Future Work

Despite the improvements mentioned in Section 4.2, the individual models still face considerable uncertainty. Concerning the total carbon sink, the OCO-2 v9 MIP and OCO-2 v10 MIP exhibit considerable spreads among the different inversions in the MIPs. Meanwhile, the GCAS OCO-2 inversion and CAMS FT21r2 inversion fall within the range of the MIP inversions but on the lower limit (Figure 9). The variations between the OCO-2 XCO<sub>2</sub> inversions may arise from XCO<sub>2</sub> retrieval uncertainties, transport models (Basu et al., 2018; Schuh et al., 2019), prior biosphere fluxes (Philip et al., 2019; L. Zhang et al., 2023), imposed component fluxes, error models, and inversion system configurations. The uncertainty of XCO<sub>2</sub> retrievals is fundamentally critical in determining the sensitivities of XCO<sub>2</sub> variations to biosphere fluxes. In addition, transport model uncertainties needed to be accounted for: it was reported that the estimates between two kinds of transport models (i.e., GEOS-Chem vs. TM5) differ as large as 0.7 PgC/yr in China in the OCO-2 v9 MIP (Schuh et al., 2022).

Here we highlight the importance of model intercomparison for inversions focusing on regional carbon budgets, such as the RECCAP-II initiative (Ciais et al., 2022) and the EUROCOM project (Monteil et al., 2020). In



the future, an inverse model intercomparison campaign focusing on the Chinese carbon sink estimate would be useful. This could be enhanced through close cooperation with international research groups, such as the OCO-2 MIP Science Team. Both the in situ CO<sub>2</sub> data and the satellite XCO<sub>2</sub> data (OCO-2 XCO<sub>2</sub>) should be employed to understand uncertainties due to data sources (possible uncertainties in XCO<sub>2</sub> retrievals). In addition, it is crucial to allocate sufficient resources toward establishing reasonable prior biosphere fluxes. This is particularly important for estimating carbon fluxes at a fine scale and in regions where CO<sub>2</sub> observations are limited. Conducting intercomparison efforts like this would help to better comprehend the uncertainties associated with inverse models as mentioned above.

## 5. Conclusions

We have investigated the constraints imposed by OCO-2 XCO<sub>2</sub> retrievals on the recent terrestrial carbon exchange over China, using an ensemble of OCO-2 inversions. The main findings are as follows:

1. Different OCO-2 inversions consistently reveal that the largest annual carbon sink is in the south of China, while the greatest carbon sink in the peak growing season is in the northeast and other main agricultural areas; this is consistent with the distribution of main forests and crops, respectively.
2. The OCO-2 inverse model amplitude of the seasonal cycle of NBP is obviously larger than bottom-up biosphere model simulations, and slightly greater than in situ inversions. More importantly, the seasonal cycle of the OCO-2 inversions appears to be plausible and informative across climate zones and ecosystems, with improvements in cross-model consistency and better correlations with multi-year mean seasonal cycles of SIF and LAI at a sub-regional scale compared to an ensemble of in situ inversions and biosphere model simulations.
3. The estimated NBP in China for 2015–2019 is between 0.34 PgC/yr (GCAS inversion) and  $0.47 \pm 0.16$  PgC/yr (median  $\pm$  std, OCO-2 v10 MIP); an ability to indicate the impact of climate extremes on NBP interannual variations is shown. A strong carbon sink reduction appears in 2019 due to drought impact, which is largely contributed by the grass and crop ecosystems that are mainly located in the TCC zone and the temperate monsoon climate zone.

Our results suggest that the assimilation of OCO-2 XCO<sub>2</sub> retrievals is effective in improving our understanding of the spatiotemporal characteristics of the terrestrial carbon balance at regional scales.

## Data Availability Statement

The GCAS v2 carbon fluxes are publicly available in the Zenodo repository (W. He, Jiang, & Ju, 2022). The CAMS carbon fluxes are available in the Copernicus Data Store (Copernicus Atmosphere Monitoring Service, 2022). OCO-2 MIP fluxes are available on the official website of the NOAA/ESRL Global Monitoring Laboratory (NOAA/ESRL Global Monitoring Laboratory, 2022). The CarbonTracker 2019B carbon flux data are publicly available on the FTP server for the CarbonTracker project (Jacobson et al., 2020; NOAA/ESRL Global Monitoring Laboratory, 2021). The CarbonTracker Europe 2020 carbon flux data are available on the FTP server for the CarbonTracker Europe project with required registration (Wageningen University & ICOS Netherlands, 2021). The Jena CarboScope carbon flux data are available on the official website for the Jena CarboScope project (Rödenbeck, 2022). The TRENDY v9 carbon fluxes are available on the official website for the TRENDY project with required registration (The TRENDY Team, 2020). The GLOBMAP v3 LAI is publicly available in the Zenodo repository (J. Liu et al., 2021; R. Liu et al., 2021). The GLASS FAPAR is publicly available on the official website for the GLASS project (Liang et al., 2020). The GLEAM v3.5 surface SM is publicly available on the official website for the GLEAM project (Martens et al., 2021). The CSIF v2 data is publicly available in the OSF repository (Y. Zhang, 2022).

## References

- Baker, D. F., Bösch, H., Doney, S. C., O'Brien, D., & Schimel, D. S. (2010). Carbon source/sink information provided by column CO<sub>2</sub> measurements from the Orbiting Carbon Observatory. *Atmospheric Chemistry and Physics*, 10(9), 4145–4165. <https://doi.org/10.5194/acp-10-4145-2010>
- Baker, D. F., Doney, S. C., & Schimel, D. S. (2006). Variational data assimilation for atmospheric CO<sub>2</sub>. *Tellus B: Chemical and Physical Meteorology*, 58(5), 359–365. <https://doi.org/10.1111/j.1600-0889.2006.00218.x>
- Basu, S., Baker, D. F., Chevallier, F., Patra, P. K., Liu, J., & Miller, J. B. (2018). The impact of transport model differences on CO<sub>2</sub> surface flux estimates from OCO-2 retrievals of column average CO<sub>2</sub>. *Atmospheric Chemistry and Physics*, 18(10), 7189–7215. <https://doi.org/10.5194/acp-18-7189-2018>

### Acknowledgments

This research is funded by the National Key R&D Program of China (Grant 2020YFA0607504), the National Natural Science Foundation of China (Grants 41907378, 42277453 and 42111530184), and the Research Funds for the Frontiers Science Center for Critical Earth Material Cycling, Nanjing University (Grant 090414380031). Matthew Johnson's contribution was supported by NASA's Carbon Cycle Science Program (Grant 80HQTR21T0101). David Baker's contribution, as well as that of the broader OCO-2 MIP activities, was supported by NASA (Grant 80NSSC18K0909). We sincerely acknowledge all model contributors of the OCO-2 MIP activities. We sincerely acknowledge all model contributors of the TRENDY v9 project. We thank Yang Shen from Nanjing University for the help with graph making. We sincerely thank the three anonymous reviewers for their detailed comments, which helped improve the paper considerably. We also gratefully acknowledge the High-Performance Computing Center (HPCC) of Nanjing University for doing the numerical calculations in this paper on its blade cluster system.

- Basu, S., Guerlet, S., Butz, A., Houweling, S., Hasekamp, O., Aben, I., et al. (2013). Global CO<sub>2</sub> fluxes estimated from GOSAT retrievals of total column CO<sub>2</sub>. *Atmospheric Chemistry and Physics*, *13*(17), 8695–8717. <https://doi.org/10.5194/acp-13-8695-2013>
- Byrne, B., Baker, D. F., Basu, S., Bertolacci, M., Bowman, K. W., Carroll, D., et al. (2023). National CO<sub>2</sub> budgets (2015–2020) inferred from atmospheric CO<sub>2</sub> observations in support of the global stocktake. *Earth System Science Data*, *15*(2), 963–1004. <https://doi.org/10.5194/essd-15-963-2023>
- Cavallaro, N., Shrestha, G., Birdsey, R., Mayes, M. A., Najjar, R. G., Reed, S. C., et al. (2018). Second state of the carbon cycle report (SOCCR2): A sustained assessment report. Retrieved from <https://carbon2018.globalchange.gov/>
- Celis, G., Mauritz, M., Bracho, R., Salmon, V. G., Webb, E. E., Hutchings, J., et al. (2017). Tundra is a consistent source of CO<sub>2</sub> at a site with progressive permafrost thaw during 6 years of chamber and eddy covariance measurements. *Journal of Geophysical Research: Biogeosciences*, *122*(6), 1471–1485. <https://doi.org/10.1002/2016JG003671>
- Chen, J. M., Ju, W., Ciais, P., Viovy, N., Liu, R., Liu, Y., & Lu, X. (2019). Vegetation structural change since 1981 significantly enhanced the terrestrial carbon sink. *Nature Communications*, *10*(1), 4259. <https://doi.org/10.1038/s41467-019-12257-8>
- Chen, J. M., Liu, J., Cihlar, J., & Goulden, M. L. (1999). Daily canopy photosynthesis model through temporal and spatial scaling for remote sensing applications. *Ecological Modelling*, *124*(2), 99–119. [https://doi.org/10.1016/s0304-3800\(99\)00156-8](https://doi.org/10.1016/s0304-3800(99)00156-8)
- Chen, Z., Huntzinger, D. N., Liu, J., Piao, S., Wang, X., Sitch, S., et al. (2021). Five years of variability in the global carbon cycle: Comparing an estimate from the orbiting carbon observatory-2 and process-based models. *Environmental Research Letters*, *16*(5), 054041. <https://doi.org/10.1088/1748-9326/abfac1>
- Chen, Z., Liu, J., Henze, D. K., Huntzinger, D. N., Wells, K. C., Sitch, S., et al. (2021). Linking global terrestrial CO<sub>2</sub> fluxes and environmental drivers: Inferences from the orbiting carbon observatory 2 satellite and terrestrial biospheric models. *Atmospheric Chemistry and Physics*, *21*(9), 6663–6680. <https://doi.org/10.5194/acp-21-6663-2021>
- Chevallier, F., Ciais, P., Conway, T. J., Aalto, T., Anderson, B. E., Bousquet, P., et al. (2010). CO<sub>2</sub> surface fluxes at grid point scale estimated from a global 21 year reanalysis of atmospheric measurements. *Journal of Geophysical Research*, *115*(D21), D21307. <https://doi.org/10.1029/2010JD013887>
- Chevallier, F., Fisher, M., Peylin, P., Serrar, S., Bousquet, P., Bréon, F.-M., et al. (2005). Inferring CO<sub>2</sub> sources and sinks from satellite observations: Method and application to TOVS data. *Journal of Geophysical Research*, *110*(D24), D24309. <https://doi.org/10.1029/2005JD006390>
- Chevallier, F., Maksyutov, S., Bousquet, P., Bréon, F. M., Saito, R., Yoshida, Y., & Yokota, T. (2009). On the accuracy of the CO<sub>2</sub> surface fluxes to be estimated from the GOSAT observations. *Geophysical Research Letters*, *36*(19), L19807. <https://doi.org/10.1029/2009gl040108>
- Chevallier, F., Remaud, M., O'Dell, C. W., Baker, D., Peylin, P., & Cozic, A. (2019). Objective evaluation of surface- and satellite-driven carbon dioxide atmospheric inversions. *Atmospheric Chemistry and Physics*, *19*(22), 14233–14251. <https://doi.org/10.5194/acp-19-14233-2019>
- Ciais, P., Bastos, A., Chevallier, F., Lauerwald, R., Poulter, B., Canadell, J. G., et al. (2022). Definitions and methods to estimate regional land carbon fluxes for the second phase of the REgional Carbon Cycle Assessment and Processes Project (RECCAP-2). *Geoscientific Model Development*, *15*(3), 1289–1316. <https://doi.org/10.5194/gmd-15-1289-2022>
- Copernicus Atmosphere Monitoring Service. (2022). CAMS global inversion-optimised greenhouse gas fluxes and concentrations [Dataset]. Retrieved from <https://ads.atmosphere.copernicus.eu/cdsapp#/dataset/cams-global-greenhouse-gas-inversion?tab=form>
- Crisp, D., Dolman, H., Tanhua, T., McKinley, G. A., Hauck, J., Bastos, A., et al. (2022). How well do we understand the land-ocean-atmosphere carbon cycle? *Reviews of Geophysics*, *60*(2), e2021RG000736. <https://doi.org/10.1029/2021RG000736>
- Crowell, S., Baker, D., Schuh, A., Basu, S., Jacobson, A. R., Chevallier, F., et al. (2019). The 2015–2016 carbon cycle as seen from OCO-2 and the global in situ network. *Atmospheric Chemistry and Physics*, *19*(15), 9797–9831. <https://doi.org/10.5194/acp-19-9797-2019>
- Delire, C., Séférian, R., Decharme, B., Alkama, R., Calvet, J.-C., Carrer, D., et al. (2020). The global land carbon cycle simulated with ISBA-CTRIP: Improvements over the last decade. *Journal of Advances in Modeling Earth Systems*, *12*(9), e2019MS001886. <https://doi.org/10.1029/2019MS001886>
- Deng, F., Jones, D. B. A., Henze, D. K., Bousseret, N., Bowman, K. W., Fisher, J. B., et al. (2014). Inferring regional sources and sinks of atmospheric CO<sub>2</sub> from GOSAT XCO<sub>2</sub> data. *Atmospheric Chemistry and Physics*, *14*(7), 3703–3727. <https://doi.org/10.5194/acp-14-3703-2014>
- Deng, F., Jones, D. B. A., O'Dell, C. W., Nassar, R., & Parazoo, N. C. (2016). Combining GOSAT XCO<sub>2</sub> observations over land and ocean to improve regional CO<sub>2</sub> flux estimates. *Journal of Geophysical Research: Atmospheres*, *121*(4), 1896–1913. <https://doi.org/10.1002/2015JD024157>
- Emmons, L. K., Walters, S., Hess, P. G., Lamarque, J. F., Pfister, G. G., Fillmore, D., et al. (2010). Description and evaluation of the model for ozone and related chemical tracers, version 4 (MOZART-4). *Geoscientific Model Development*, *3*(1), 43–67. <https://doi.org/10.5194/gmd-3-43-2010>
- Fan, S., Gloor, M., Mahlman, J., Pacala, S., Sarmiento, J., Takahashi, T., & Tans, P. (1998). A large terrestrial carbon sink in North America implied by atmospheric and oceanic carbon dioxide data and models. *Science*, *282*(5388), 442–446. <https://doi.org/10.1126/science.282.5388.442>
- Fang, J., Yu, G., Liu, L., Hu, S., & Chapin, F. S. (2018). Climate change, human impacts, and carbon sequestration in China. *Proceedings of the National Academy of Sciences of the United States of America*, *115*(16), 4015–4020. <https://doi.org/10.1073/pnas.1700304115>
- Field, C. B., & Fung, I. Y. (1999). The not-so-big U.S. carbon sink. *Science*, *285*(5427), 544–545. <https://doi.org/10.1126/science.285.5427.544>
- Foley, J. A., Prentice, I. C., Ramankutty, N., Levis, S., Pollard, D., Sitch, S., & Haxeltine, A. (1996). An integrated biosphere model of land surface processes, terrestrial carbon balance, and vegetation dynamics. *Global Biogeochemical Cycles*, *10*(4), 603–628. <https://doi.org/10.1029/96GB02692>
- Friedlingstein, P., Jones, M. W., O'Sullivan, M., Andrew, R. M., Bakker, D. C. E., Hauck, J., et al. (2022). Global carbon budget 2021. *Earth System Science Data*, *14*(4), 1917–2005. <https://doi.org/10.5194/essd-14-1917-2022>
- Friedlingstein, P., O'Sullivan, M., Jones, M. W., Andrew, R. M., Hauck, J., Olsen, A., et al. (2020). Global carbon budget 2020. *Earth System Science Data*, *12*(4), 3269–3340. <https://doi.org/10.5194/essd-12-3269-2020>
- Guanter, L., Zhang, Y., Jung, M., Joiner, J., Voigt, M., Berry, J. A., et al. (2014). Global and time-resolved monitoring of crop photosynthesis with chlorophyll fluorescence. *Proceedings of the National Academy of Sciences of the United States of America*, *111*(14), 1327–1333. <https://doi.org/10.1073/pnas.132008111>
- Gurney, K. R., Law, R. M., Denning, A. S., Rayner, P. J., Pak, B. C., Baker, D., et al. (2004). Transcom 3 inversion intercomparison: Model mean results for the estimation of seasonal carbon sources and sinks. *Global Biogeochemical Cycles*, *18*(1), GB1010. <https://doi.org/10.1029/2003GB002111>
- Haverd, V., Smith, B., Nieradzic, L., Briggs, P. R., Woodgate, W., Trudinger, C. M., et al. (2018). A new version of the CABLE land surface model (Subversion revision r4601) incorporating land use and land cover change, woody vegetation demography, and a novel optimisation-based approach to plant coordination of photosynthesis. *Geoscientific Model Development*, *11*(7), 2995–3026. <https://doi.org/10.5194/gmd-11-2995-2018>

- He, L., Chen, J. M., Pisek, J., Schaaf, C. B., & Strahler, A. H. (2012). Global clumping index map derived from the MODIS BRDF product. *Global clumping index map derived from the MODIS BRDF product. Remote Sensing of Environment*, 119, 118–130. <https://doi.org/10.1016/j.rse.2011.12.008>
- He, W., Jiang, F., & Ju, W. (2022). Global net ecosystem exchange of CO<sub>2</sub> inferred from the OCO-2 XCO<sub>2</sub> retrievals (GCAS OCO-2 inversion) [Dataset]. Zenodo. <https://doi.org/10.5281/zenodo.7040223>
- He, W., Jiang, F., Ju, W., Byrne, B., Xiao, J., Nguyen, N. T., et al. (2023). Do state-of-the-art atmospheric CO<sub>2</sub> inverse models capture drought impacts on the European land carbon uptake? *Journal of Advances in Modeling Earth Systems*, 15(6), e2022MS003150. <https://doi.org/10.1029/2022MS003150>
- He, W., Jiang, F., Wu, M., Ju, W., Scholze, M., Chen, J. M., et al. (2022). China's terrestrial carbon sink over 2010–2015 constrained by satellite observations of atmospheric CO<sub>2</sub> and land surface variables. *Journal of Geophysical Research: Biogeosciences*, 127(2), e2021JG006644. <https://doi.org/10.1029/2021JG006644>
- He, W., Ju, W., Jiang, F., Parazoo, N., Gentine, P., Wu, X., et al. (2021). Peak growing season patterns and climate extremes-driven responses of gross primary production estimated by satellite and process based models over North America. *Agricultural and Forest Meteorology*, 298, 108292. <https://doi.org/10.1016/j.agrformet.2020.108292>
- He, W., Ju, W., Schwalm, C. R., Sippel, S., Wu, X., He, Q., et al. (2018a). Large-scale droughts responsible for dramatic reductions of terrestrial net carbon uptake over North America in 2011 and 2012. *Journal of Geophysical Research: Biogeosciences*, 123(7), 2053–2071. <https://doi.org/10.1029/2018jg004520>
- He, W., Velde, I. R., Andrews, A. E., Sweeney, C., Miller, J., Tans, P., et al. (2018b). CTDAS-Lagrange v1. 0: A high-resolution data assimilation system for regional carbon dioxide observations. *Geoscientific Model Development*, 11(8), 3515–3536. <https://doi.org/10.5194/gmd-11-3515-2018>
- Hilton, T. W., Whelan, M. E., Zumkehr, A., Kulkarni, S., Berry, J. A., Baker, I. T., et al. (2017). Peak growing season gross uptake of carbon in North America is largest in the midwest USA. *Nature Climate Change*, 7(6), 450–454. <https://doi.org/10.1038/nclimate3272>
- Holland, E., & Brown, S. A. (1999). North American carbon sink. *Science*, 283(5409), 1813. <https://doi.org/10.1126/science.283.5409.1815a>
- Jacobson, A. R., Schuldt, K. N., Miller, J. B., Oda, T., Tans, P., Arlyn, A., et al. (2020). *CarbonTracker CT2019B*. NOAA Global Monitoring Laboratory.
- Jain, A. K., Meiyappan, P., Song, Y., & House, J. I. (2013). CO<sub>2</sub> emissions from land-use change affected more by nitrogen cycle, than by the choice of land-cover data. *Global Change Biology*, 19(9), 2893–2906. <https://doi.org/10.1111/gcb.12207>
- Janssens, I. A., Freibauer, A., Ciais, P., Smith, P., Nabuurs, G.-J., Folberth, G., et al. (2003). Europe's terrestrial biosphere absorbs 7 to 12% of European anthropogenic CO<sub>2</sub> emissions. *Science*, 300(5625), 1538–1542. <https://doi.org/10.1126/science.1083592>
- Jiang, F. (2022). A ten-year global monthly averaged terrestrial NEE inferred from the ACOS GOSAT v9 CO<sub>2</sub> retrievals (GCAS2021) [Dataset]. <https://doi.org/10.5281/zenodo.5829774>
- Jiang, F., Chen, J. M., Zhou, L., Ju, W., Zhang, H., Machida, T., et al. (2016). A comprehensive estimate of recent carbon sinks in China using both top-down and bottom-up approaches. *Scientific Reports*, 6(1), 22130. <https://doi.org/10.1038/srep22130>
- Jiang, F., He, W., Ju, W., Wang, H., Wu, M., Wang, J., et al. (2022). The status of carbon neutrality of the world's top 5 CO<sub>2</sub> emitters as seen by carbon satellites. *Fundamental Research*, 2(3), 357–366. <https://doi.org/10.1016/j.fmre.2022.02.001>
- Jiang, F., Ju, W., He, W., Wu, M., Wang, H., Wang, J., et al. (2022). A ten-year global monthly averaged terrestrial NEE inferred from the ACOS GOSAT v9 CO<sub>2</sub> retrievals (GCAS2021). *Earth System Science Data*, 14(7), 3013–3037. <https://doi.org/10.5194/essd-14-3013-2022>
- Jiang, F., Wang, H., Chen, J. M., Ju, W., Tian, X., Feng, S., et al. (2021). Regional CO<sub>2</sub> fluxes from 2010 to 2015 inferred from GOSAT XCO<sub>2</sub> retrievals using a new version of the Global Carbon Assimilation System. *Atmospheric Chemistry and Physics*, 21(3), 1963–1985. <https://doi.org/10.5194/acp-21-1963-2021>
- Jones, M. W., Andrew, R. M., Peters, G. P., Janssens-Maenhout, G., De-Gol, A. J., Ciais, P., et al. (2021). Gridded fossil CO<sub>2</sub> emissions and related O<sub>2</sub> combustion consistent with national inventories 1959–2018. *Scientific Data*, 8(1), 2. <https://doi.org/10.1038/s41597-020-00779-6>
- Ju, W., Chen, J. M., Black, T. A., Barr, A. G., Liu, J., & Chen, B. (2006). Modelling multi-year coupled carbon and water fluxes in a boreal aspen forest. *Agricultural and Forest Meteorology*, 140(1), 136–151. <https://doi.org/10.1016/j.agrformet.2006.08.008>
- Kiel, M., O'Dell, C. W., Fisher, B., Eldering, A., Nassar, R., MacDonald, C. G., & Wennberg, P. O. (2019). How bias correction goes wrong: Measurement of XCO<sub>2</sub> affected by erroneous surface pressure estimates. *Atmospheric Measurement Techniques*, 12(4), 2241–2259. <https://doi.org/10.5194/amt-12-2241-2019>
- Krinner, G., Viovy, N., de Noblet-Ducoudré, N., Ogée, J., Polcher, J., Friedlingstein, P., et al. (2005). A dynamic global vegetation model for studies of the coupled atmosphere-biosphere system. *Global Biogeochemical Cycles*, 19(1), GB1015. <https://doi.org/10.1029/2003gb002199>
- Kwon, M. J., Ballantyne, A., Ciais, P., Bastos, A., Chevallier, F., Liu, Z., et al. (2021). Siberian 2020 heatwave increased spring CO<sub>2</sub> uptake but not annual CO<sub>2</sub> uptake. *Environmental Research Letters*, 16(12), 124030. <https://doi.org/10.1088/1748-9326/ac358b>
- Li, X., Xiao, J., He, B., Altaf Arain, M., Beringer, J., Desai, A. R., et al. (2018). Solar-induced chlorophyll fluorescence is strongly correlated with terrestrial photosynthesis for a wide variety of biomes: First global analysis based on OCO-2 and flux tower observations. *Global Change Biology*, 24(9), 3990–4008. <https://doi.org/10.1111/gcb.14297>
- Liang, S., Cheng, C., Jia, K., Jiang, B., Liu, Q., Xiao, Z., et al. (2020). The global land surface satellite (GLASS) product suite: Fraction of absorbed photosynthetically active radiation (FAPAR) (version V60) [Dataset]. Retrieved from <http://www.glass.umd.edu/Download.html>
- Lienert, S., & Joos, F. (2018). A Bayesian ensemble data assimilation to constrain model parameters and land-use carbon emissions. *Biogeosciences*, 15(9), 2909–2930. <https://doi.org/10.5194/bg-15-2909-2018>
- Liu, J., Baskaran, L., Bowman, K., Schimel, D., Bloom, A. A., Parazoo, N. C., et al. (2021). Carbon monitoring system flux net biosphere exchange 2020 (CMS-Flux NBE 2020). *Earth System Science Data*, 13(2), 299–330. <https://doi.org/10.5194/essd-13-299-2021>
- Liu, R., Liu, Y., & Chen, J. M. (2021). GLOBMAP global leaf area index since 1981 [Dataset]. Zenodo. <https://doi.org/10.5281/zenodo.4700264>
- Liu, Y., Liu, R., & Chen, J. M. (2012). Retrospective retrieval of long-term consistent global leaf area index (1981–2011) from combined AVHRR and MODIS data. *Journal of Geophysical Research*, 117(G4), G04003. <https://doi.org/10.1029/2012JG002084>
- Liu, Z., Zeng, N., Liu, Y., Kalnay, E., Asrar, G., Wu, B., et al. (2022). Improving the joint estimation of CO<sub>2</sub> and surface carbon fluxes using a constrained ensemble Kalman filter in COLA (v1.0). *Geoscientific Model Development*, 15(14), 5511–5528. <https://doi.org/10.5194/gmd-15-5511-2022>
- Ma, S., Zhu, C., & Liu, J. (2020). Combined impacts of warm central equatorial Pacific sea surface temperatures and anthropogenic warming on the 2019 severe drought in East China. *Advances in Atmospheric Sciences*, 37(11), 1149–1163. <https://doi.org/10.1007/s00376-020-0077-8>
- Machida, T., Matsueda, H., Sawa, Y., Nakagawa, Y., Hirofani, K., Kondo, N., et al. (2008). Worldwide measurements of atmospheric CO<sub>2</sub> and other trace gas species using commercial airlines. *Journal of Atmospheric and Oceanic Technology*, 25(10), 1744–1754. <https://doi.org/10.1175/2008JTECHA1082.1>

- Maksyutov, S., Oda, T., Saito, M., Janardanan, R., Belikov, D., Kaiser, J. W., et al. (2021). Technical note: A high-resolution inverse modelling technique for estimating surface CO<sub>2</sub> fluxes based on the NIES-TM-FLEXPART coupled transport model and its adjoint. *Atmospheric Chemistry and Physics*, 21(2), 1245–1266. <https://doi.org/10.5194/acp-21-1245-2021>
- Martens, B., Miralles, D. G., Lievens, H., van der Schalie, R., de Jeu, R. A. M., Fernández-Prieto, D., et al. (2017). GLEAM v3: Satellite-based land evaporation and root-zone soil moisture. *Geoscientific Model Development*, 10(5), 1903–1925. <https://doi.org/10.5194/gmd-10-1903-2017>
- Martens, B., Miralles, D. G., Lievens, H., van der Schalie, R., de Jeu, R. A. M., Fernández-Prieto, D., et al. (2021). The global land evaporation Amsterdam model v3.5 surface soil moisture [Dataset]. Retrieved from <https://www.gleam.eu/#downloads>
- Masarie, K. A., Peters, W., Jacobson, A. R., & Tans, P. P. (2014). ObsPack: A framework for the preparation, delivery, and attribution of atmospheric greenhouse gas measurements. *Earth System Science Data*, 6(2), 375–384. <https://doi.org/10.5194/essd-6-375-2014>
- Melton, J. R., Arora, V. K., Wisernig-Cojoc, E., Seiler, C., Fortier, M., Chan, E., & Teckentrup, L. (2020). CLASSIC v1.0: The open-source community successor to the Canadian land surface scheme (CLASS) and the Canadian terrestrial ecosystem model (CTEM) – Part 1: Model framework and site-level performance. *Geoscientific Model Development*, 13(6), 2825–2850. <https://doi.org/10.5194/gmd-13-2825-2020>
- Miller, S. M., Saibaba, A. K., Trudeau, M. E., Mountain, M. E., & Andrews, A. E. (2020). Geostatistical inverse modeling with very large datasets: An example from the orbiting carbon observatory 2 (OCO-2) satellite. *Geoscientific Model Development*, 13(3), 1771–1785. <https://doi.org/10.5194/gmd-13-1771-2020>
- Miralles, D. G., Holmes, T. R. H., De Jeu, R. A. M., Gash, J. H., Meesters, A. G. C. A., & Dolman, A. J. (2011). Global land-surface evaporation estimated from satellite-based observations. *Hydrology and Earth System Sciences*, 15(2), 453–469. <https://doi.org/10.5194/hess-15-453-2011>
- Monteil, G., Broquet, G., Scholze, M., Lang, M., Karstens, U., Gerbig, C., et al. (2020). The regional European atmospheric transport inversion comparison, EUROCOM: First results on European-wide terrestrial carbon fluxes for the period 2006–2015. *Atmospheric Chemistry and Physics*, 20(20), 12063–12091. <https://doi.org/10.5194/acp-20-12063-2020>
- NOAA/ESRL Global Monitoring Laboratory. (2021). The OCO-2 v10 MIP [Dataset]. Retrieved from [https://gml.noaa.gov/ccgg/OCO2\\_v10mip/download.php](https://gml.noaa.gov/ccgg/OCO2_v10mip/download.php)
- NOAA/ESRL Global Monitoring Laboratory. (2022). CarbonTracker CT2019B [Dataset]. Retrieved from <https://gml.noaa.gov/aftp/products/carbontracker/co2/>
- O'Dell, C. W., Eldering, A., Wennberg, P. O., Crisp, D., Gunson, M. R., Fisher, B., et al. (2018). Improved retrievals of carbon dioxide from Orbiting Carbon Observatory-2 with the version 8 ACOS algorithm. *Atmospheric Measurement Techniques*, 11(12), 6539–6576. <https://doi.org/10.5194/amt-11-6539-2018>
- Peiro, H., Crowell, S., Schuh, A., Baker, D. F., O'Dell, C., Jacobson, A. R., et al. (2022). Four years of global carbon cycle observed from the Orbiting Carbon Observatory 2 (OCO-2) version 9 and in situ data and comparison to OCO-2 version 7. *Atmospheric Chemistry and Physics*, 22(2), 1097–1130. <https://doi.org/10.5194/acp-22-1097-2022>
- Peters, W., Jacobson, A. R., Sweeney, C., Andrews, A. E., Conway, T. J., Masarie, K., et al. (2007). An atmospheric perspective on North American carbon dioxide exchange: CarbonTracker. *Proceedings of the National Academy of Sciences of the United States of America*, 104(48), 18925–18930. <https://doi.org/10.1073/pnas.0708986104>
- Peters, W., Krol, M., Van Der Werf, G., Houweling, S., Jones, C., Hughes, J., et al. (2010). Seven years of recent European net terrestrial carbon dioxide exchange constrained by atmospheric observations. *Global Change Biology*, 16(4), 1317–1337. <https://doi.org/10.1111/j.1365-2486.2009.02078.x>
- Peters, W., Miller, J. B., Whitaker, J., Denning, A. S., Hirsch, A., Krol, M. C., et al. (2005). An ensemble data assimilation system to estimate CO<sub>2</sub> surface fluxes from atmospheric trace gas observations. *Journal of Geophysical Research*, 110(D24), D24304. <https://doi.org/10.1029/2005jd006157>
- Peylin, P., Law, R., Gurney, K., Chevallier, F., Jacobson, A., Maki, T., et al. (2013). Global atmospheric carbon budget: Results from an ensemble of atmospheric CO<sub>2</sub> inversions. *Biogeosciences*, 10, 6699–6720. <https://doi.org/10.5194/bg-10-6699-2013>
- Philip, S., Johnson, M. S., Baker, D. F., Basu, S., Tiwari, Y. K., Indira, N. K., et al. (2022). OCO-2 satellite-imposed constraints on terrestrial biospheric CO<sub>2</sub> fluxes over south Asia. *Journal of Geophysical Research: Atmospheres*, 127(3), e2021JD035035. <https://doi.org/10.1029/2021JD035035>
- Philip, S., Johnson, M. S., Potter, C., Genovesse, V., Baker, D. F., Haynes, K. D., et al. (2019). Prior biosphere model impact on global terrestrial CO<sub>2</sub> fluxes estimated from OCO-2 retrievals. *Atmospheric Chemistry and Physics*, 19(20), 13267–13287. <https://doi.org/10.5194/acp-19-13267-2019>
- Piao, S., Fang, J., Ciais, P., Peylin, P., Huang, Y., Sitch, S., & Wang, T. (2009). The carbon balance of terrestrial ecosystems in China. *Nature*, 458(7241), 1009–1013. <https://doi.org/10.1038/nature07944>
- Piao, S., He, Y., Wang, X., & Chen, F. (2022). Estimation of China's terrestrial ecosystem carbon sink: Methods, progress and prospects. *Science China Earth Sciences*, 65(4), 641–651. <https://doi.org/10.1007/s11430-021-9892-6>
- Poulter, B., Frank, D. C., Hodson, E. L., & Zimmermann, N. E. (2011). Impacts of land cover and climate data selection on understanding terrestrial carbon dynamics and the CO<sub>2</sub> airborne fraction. *Biogeosciences*, 8(8), 2027–2036. <https://doi.org/10.5194/bg-8-2027-2011>
- Reuter, M., Buchwitz, M., Hilker, M., Heymann, J., Bovensmann, H., Burrows, J. P., et al. (2017). How much CO<sub>2</sub> is taken up by the European terrestrial biosphere? *Bulletin of the American Meteorological Society*, 98(4), 665–671. <https://doi.org/10.1175/bams-d-15-00310.1>
- Rödenbeck, C. (2022). Jena CarboScope atmospheric CO<sub>2</sub> inversion [Dataset]. Retrieved from <http://www.bgc-jena.mpg.de/CarboScope/>
- Rödenbeck, C., Houweling, S., Gloor, M., & Heimann, M. (2003). CO<sub>2</sub> flux history 1982–2001 inferred from atmospheric data using a global inversion of atmospheric transport. *Atmospheric Chemistry and Physics*, 3(6), 1919–1964. <https://doi.org/10.5194/acp-3-1919-2003>
- Rödenbeck, C., Zaehle, S., Keeling, R., & Heimann, M. (2018). How does the terrestrial carbon exchange respond to inter-annual climatic variations? A quantification based on atmospheric CO<sub>2</sub> data. *Biogeosciences*, 15(8), 2481–2498. <https://doi.org/10.5194/bg-15-2481-2018>
- Scholze, M., Kaminski, T., Knorr, W., Voßbeck, M., Wu, M., Ferrazzoli, P., et al. (2019). Mean European carbon sink over 2010–2015 estimated by simultaneous assimilation of atmospheric CO<sub>2</sub>, soil moisture, and vegetation optical depth. *Geophysical Research Letters*, 46(23), 13796–13803. <https://doi.org/10.1029/2019GL085725>
- Schuh, A. E., Byrne, B., Jacobson, A. R., Crowell, S. M. R., Deng, F., Baker, D. F., et al. (2022). On the role of atmospheric model transport uncertainty in estimating the Chinese land carbon sink. *Nature*, 603(7901), E13–E14. <https://doi.org/10.1038/s41586-021-04258-9>
- Schuh, A. E., Jacobson, A. R., Basu, S., Weir, B., Baker, D., Bowman, K., et al. (2019). Quantifying the impact of atmospheric transport uncertainty on CO<sub>2</sub> surface flux estimates. *Global Biogeochemical Cycles*, 33(4), 484–500. <https://doi.org/10.1029/2018GB006086>
- Schuh, A. E., Lauvaux, T., West, T. O., Denning, A. S., Davis, K. J., Miles, N., et al. (2013). Evaluating atmospheric CO<sub>2</sub> inversions at multiple scales over a highly inventoried agricultural landscape. *Global Change Biology*, 19(5), 1424–1439. <https://doi.org/10.1111/gcb.12141>
- Schuur, E. A. G., Bracho, R., Celis, G., Belshe, E. F., Ebert, C., Ledman, J., et al. (2021). Tundra underlain by thawing permafrost persistently emits carbon to the atmosphere over 15 years of measurements. *Journal of Geophysical Research: Biogeosciences*, 126(6), e2020JG006044. <https://doi.org/10.1029/2020JG006044>

- Sitch, S., Friedlingstein, P., Gruber, N., Jones, S., Murray-Tortarolo, G., Ahlström, A., et al. (2015). Recent trends and drivers of regional sources and sinks of carbon dioxide. *Biogeosciences*, *12*(3), 653–679. <https://doi.org/10.5194/bg-12-653-2015>
- Sun, W., Fang, Y., Luo, X., Shiga, Y. P., Zhang, Y., Andrews, A. E., et al. (2021). Midwest US croplands determine model divergence in North American carbon fluxes. *AGU Advances*, *2*(2), e2020AV000310. <https://doi.org/10.1029/2020AV000310>
- Sun, Y., Goll, D. S., Chang, J., Ciais, P., Guenet, B., Helfenstein, J., et al. (2021). Global evaluation of the nutrient-enabled version of the land surface model ORCHIDEE-CNP v1.2 (r5986). *Geoscientific Model Development*, *14*(4), 1987–2010. <https://doi.org/10.5194/gmd-14-1987-2021>
- Takahashi, T., Sutherland, S. C., Wanninkhof, R., Sweeney, C., Feely, R. A., Chipman, D. W., et al. (2009). Climatological mean and decadal change in surface ocean pCO<sub>2</sub>, and net sea–air CO<sub>2</sub> flux over the global oceans. *Deep Sea Research Part II: Topical Studies in Oceanography*, *56*(8), 554–577. <https://doi.org/10.1016/j.dsr2.2008.12.009>
- The TRENDY Team. (2020). TRENDY: Trends in the land carbon cycle [Dataset]. Retrieved from <https://sites.exeter.ac.uk/trendy>
- Thompson, R. L., Patra, P. K., Chevallier, F., Maksyutov, S., Law, R. M., Ziehn, T., et al. (2016). Top-down assessment of the Asian carbon budget since the mid 1990s. *Nature Communications*, *7*(1), 10724. <https://doi.org/10.1038/ncomms10724>
- Tian, H., Melillo, J., Lu, C., Kicklighter, D., Liu, M., Ren, W., et al. (2011). China's terrestrial carbon balance: Contributions from multiple global change factors. *Global Biogeochemical Cycles*, *25*(1), GB1007. <https://doi.org/10.1029/2010GB003838>
- Tian, H., Xu, X., Lu, C., Liu, M., Ren, W., Chen, G., et al. (2011). Net exchanges of CO<sub>2</sub>, CH<sub>4</sub>, and N<sub>2</sub>O between China's terrestrial ecosystems and the atmosphere and their contributions to global climate warming. *Journal of Geophysical Research*, *116*(G2), G02011. <https://doi.org/10.1029/2010JG001393>
- van der Laan-Luijckx, I. T., van der Velde, I. R., van der Veen, E., Tsuruta, A., Stanislawski, K., Babenhausen, A., et al. (2017). The CarbonTracker data assimilation shell (CTDAS) v1.0: Implementation and global carbon balance 2001–2015. *Geoscientific Model Development*, *10*(7), 2785–2800. <https://doi.org/10.5194/gmd-10-2785-2017>
- van der Werf, G. R., Randerson, J. T., Giglio, L., van Leeuwen, T. T., Chen, Y., Rogers, B. M., et al. (2017). Global fire emissions estimates during 1997–2016. *Earth System Science Data*, *9*(2), 697–720. <https://doi.org/10.5194/essd-9-697-2017>
- Villalobos, Y., Rayner, P. J., Silver, J. D., Thomas, S., Haverd, V., Knauer, J., et al. (2021). Was Australia a sink or source of CO<sub>2</sub> in 2015? Data assimilation using OCO-2 satellite measurements. *Atmospheric Chemistry and Physics*, *21*(23), 17453–17494. <https://doi.org/10.5194/acp-21-17453-2021>
- Villalobos, Y., Rayner, P. J., Silver, J. D., Thomas, S., Haverd, V., Knauer, J., et al. (2022). Interannual variability in the Australian carbon cycle over 2015–2019, based on assimilation of OCO-2 satellite data. *Atmospheric Chemistry and Physics Discussions*, 1–57. Retrieved from <https://acp.copernicus.org/preprints/acp-2022-15/>
- Vuichard, N., Messina, P., Luyssaert, S., Guenet, B., Zaehle, S., Ghattas, J., et al. (2019). Accounting for carbon and nitrogen interactions in the global terrestrial ecosystem model ORCHIDEE (trunk version, rev 4999): Multi-scale evaluation of gross primary production. *Geoscientific Model Development*, *12*(11), 4751–4779. <https://doi.org/10.5194/gmd-12-4751-2019>
- Wageningen University, & ICOS Netherlands. (2021). CarbonTracker Europe 2020 [Dataset]. <https://carbontracker.eu/download.shtml>
- Wang, H., Jiang, F., Wang, J., Ju, W., & Chen, J. M. (2019). Terrestrial ecosystem carbon flux estimated using GOSAT and OCO-2 XCO<sub>2</sub> retrievals. *Atmospheric Chemistry and Physics*, *19*(18), 12067–12082. <https://doi.org/10.5194/acp-19-12067-2019>
- Wang, J., Feng, L., Palmer, P. I., Liu, Y., Fang, S., Bösch, H., et al. (2020). Large Chinese land carbon sink estimated from atmospheric carbon dioxide data. *Nature*, *586*(7831), 720–723. <https://doi.org/10.1038/s41586-020-2849-9>
- Wang, K., Wang, X., Piao, S., Chevallier, F., Mao, J., Shi, X., et al. (2021). Unusual characteristics of the carbon cycle during the 2015–2016 El Niño. *Global Change Biology*, *27*(16), 3798–3809. <https://doi.org/10.1111/gcb.15669>
- Wang, Y., Wang, X., Wang, K., Chevallier, F., Zhu, D., Lian, J., et al. (2022). The size of the land carbon sink in China. *Nature*, *603*(7901), E7–E9. <https://doi.org/10.1038/s41586-021-04255-y>
- Weir, B., Crisp, D., O'Dell, C. W., Basu, S., Chatterjee, A., Kolassa, J., et al. (2021). Regional impacts of COVID-19 on carbon dioxide detected worldwide from space. *Science Advances*, *7*(45), eabf9415. <https://doi.org/10.1126/sciadv.abf9415>
- Whitaker, J. S., & Hamill, T. M. (2002). Ensemble data assimilation without perturbed observations. *Monthly Weather Review*, *130*(7), 1913–1924. [https://doi.org/10.1175/1520-0493\(2002\)130<1913:EDAWPO>2.0.CO;2](https://doi.org/10.1175/1520-0493(2002)130<1913:EDAWPO>2.0.CO;2)
- Yang, Y., Shi, Y., Sun, W., Chang, J., Zhu, J., Chen, L., et al. (2022). Terrestrial carbon sinks in China and around the world and their contribution to carbon neutrality. *SCIENTIA SINICA Vitae*, *52*(1674–7232), 534. <https://doi.org/10.1360/SSV-2021-0362>
- Yao, Y., Li, Z., Wang, T., Chen, A., Wang, X., Du, M., et al. (2018). A new estimation of China's net ecosystem productivity based on eddy covariance measurements and a model tree ensemble approach. *Agricultural and Forest Meteorology*, *253–254*, 84–93. <https://doi.org/10.1016/j.agrformet.2018.02.007>
- Ye, X., & Chuai, X. (2022). Carbon sinks/sources' spatiotemporal evolution in China and its response to built-up land expansion. *Journal of Environmental Management*, *321*, 115863. <https://doi.org/10.1016/j.jenvman.2022.115863>
- Yu, G., Chen, Z., Piao, S., Peng, C., Ciais, P., Wang, Q., et al. (2014). High carbon dioxide uptake by subtropical forest ecosystems in the East Asian monsoon region. *Proceedings of the National Academy of Sciences of the United States of America*, *111*(13), 4910–4915. <https://doi.org/10.1073/pnas.1317065111>
- Yue, X., & Unger, N. (2015). The Yale interactive terrestrial biosphere model version 1.0: Description, evaluation and implementation into NASA GISS ModelE2. *Geoscientific Model Development*, *8*(8), 2399–2417. <https://doi.org/10.5194/gmd-8-2399-2015>
- Zaehle, S., & Friend, A. D. (2010). Carbon and nitrogen cycle dynamics in the O-CN land surface model: 1. Model description, site-scale evaluation, and sensitivity to parameter estimates. *Global Biogeochemical Cycles*, *24*(1), GB1005. <https://doi.org/10.1029/2009GB003521>
- Zammit-Mangion, A., Bertolacci, M., Fisher, J., Stavert, A., Rigby, M., Cao, Y., & Cressie, N. (2022). WOMBAT v1.0: A fully Bayesian global flux-inversion framework. *Geoscientific Model Development*, *15*(1), 45–73. <https://doi.org/10.5194/gmd-15-45-2022>
- Zhang, L., Jiang, F., He, W., Wu, M., Wang, J., Ju, W., et al. (2023). A robust estimate of continental-scale terrestrial carbon sinks using GOSAT XCO<sub>2</sub> retrievals. *Geophysical Research Letters*, *50*(6), e2023GL102815. <https://doi.org/10.1029/2023GL102815>
- Zhang, S., Zheng, X., Chen, J. M., Chen, Z., Dan, B., Yi, X., et al. (2015). A global carbon assimilation system using a modified ensemble Kalman filter. *Geoscientific Model Development*, *8*(3), 805–816. <https://doi.org/10.5194/gmd-8-805-2015>
- Zhang, Y. (2022). Contiguous solar induced chlorophyll fluorescence (CSIF). [Dataset]. OSF. <https://doi.org/10.17605/OSF.IO/8XQY6>
- Zhang, Y., Joiner, J., Alemohammad, S. H., Zhou, S., & Gentine, P. (2018). A global spatially contiguous solar-induced fluorescence (CSIF) dataset using neural networks. *Biogeosciences*, *15*(19), 5779–5800. <https://doi.org/10.5194/bg-15-5779-2018>